JOURNAL OF GEOPHYSICAL RESEARCH, VOL. 95, NO. C10, PAGES 17,921–17,945, OCTOBER 15, 1990

Observing the Tropical Atlantic Ocean in 1986–1987 From Altimetry

SABINE ARNAULT

Laboratoire d'Océanographie Dynamique et de Climatologie, ORSTOM, Université Pierre et Marie Curie, Paris

YVES MENARD

Groupe de Recherche en Géodésie Spatiale, Centre National d' Etudes Spatiales, Toulouse, France

JACQUES MERLE

Laboratoire d'Océanographie Dynamique et de Climatologie, ORSTOM, Université Pierre et Marie Curie, Paris

Geosat altimeter data from November 1986 through November 1987 are analyzed over the tropical Atlantic Ocean, between 20°N to 20°S and 60°W to 20°E, using the colinear profile method. The altimetric sea level anomalies are consistent with the large-scale signal of the tropical Atlantic as observed by historical dynamic height. The agreement in the North Equatorial Countercurrent region (around 5°N) is particularly good. Comparison of altimetric anomalies with 1986–1987 in situ data points out the part of interannual events in the explanation of the differences encountered between altimetry and climatology. Altimetric data are also compared with the results of a simple model forced with monthly 1986–1987 wind stresses. This comparison confirms and emphasizes the hypothesis of a weak and early 1987 summer upwelling in the Gulf of Guinea.

1. INTRODUCTION

During the last few decades, historical data of merchant ship BT profiles and extensive oceanographic experiments such as the GARP Atlantic Tropical Experiment (GATE) in 1974, the First GARP Global Experiment (FGGE) in 1979, and more recently the FOCAL (Programme Français Océan Climat en Atlantique Equatorial) and SEQUAL (Seasonal Response of the Equatorial Atlantic) programs in 1982–1984 have evidenced the large spectrum of the variability in the upper layers of the tropical oceans, especially in the Atlantic [*Lass et al.*, 1987; *Hisard and Hénin*, 1987; *Katz*, 1986]. However, oceanographic cruises have, for technical and funding reasons, such limited duration and spatial coverage that it is difficult to resolve large spatial and temporal scales.

Progress in modeling the tropical ocean has also been made in recent years, starting from process models [*Cane and Sarachik*, 1981; *Busalacchi and Picaut*, 1983; *Du Penhoat and Gouriou*, 1987] to more realistic and complex models [*Philander and Pacanowski*, 1986]. Recent investigations in data assimilation, in the tropical regions [*Leetmaa and Ji*, 1989; *Morlière et al.*, 1989] emphasize the crucial problem of insufficient oceanic data.

Spatial techniques give us the opportunity to have a global quasi synoptic view of the whole ocean. Three generations of altimeters (Skylab, GEOS 3, Seasat) have demonstrated the ability of altimetric data to study surface circulation [*Cheney et al.*, 1983; *Douglas et al.*, 1983; *Fu*, 1983; *Menard*, 1983]. However, most of these studies concerned the mesoscale signal, whose characteristic time-space scales are well decorrelated from the altimetric error field. Looking at the large-scale signal is more challenging because of the possible overlap by altimetric long-wavelength errors (orbit error and atmospheric and oceanic errors). However, encouraging results have been obtained in the tropical Pacific using crossover differences [*Miller et al.*, 1986] or colinear tracks [*Musman*, 1986; *Malarde et al.*, 1987] and in the Indian Ocean [*Perigaud et al.*, 1986]. More recently, in the tropical Atlantic Ocean, *Menard* [1988] found a good agreement between the seasonal variability of the dynamic topography as observed from historical hydrographic data [*Merle and Arnault*, 1985] and from GEOS 3 and Seasat altimetric data referred to a mean sea surface.

This study is pursued here by analyzing, with the colinear profile method, the data of the U.S. Navy Geosat altimeter launched in March 1985. Geosat is the first altimeter offering the opportunity of applying this method for a complete year starting in November 1986. The altimetric results over the tropical Atlantic Ocean are compared with in situ data (hydrography and inversed echo sounders (IES)). The differences are explained, through a numerical simulation, as possible artifacts or real interannual anomalies. The data processing and method are first described in section 2. Results are analyzed in sections 3 and 4. Discussions and conclusions are presented in the last section.

2. DATA PROCESSING AND METHOD

2.1. *Altimetric Data*

Launched in March 1985, the U.S. Navy Geosat altimeter performed a geodetic mission during its first 18 months of operation using a nonrepeat orbit. In November 1986 it was shifted onto a 17.05-day exact repeat orbit. The orbit tracks are separated by about 150 km at the equator. Along one track, the distance between two measurements is 7 km. We considered the Geosat exact repeat mission data over the tropical Atlantic Ocean between 60°W to 20°E and 20°N to 20°S. This data set consists of about 118 repetitive tracks of

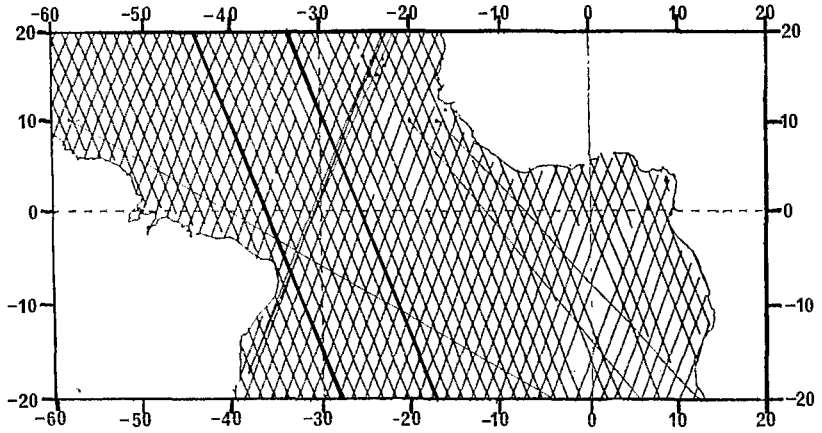

Fig. 1. Geosat data coverage between 60°W to 20°E and 20°N to 20°S for the cycle from April 27, 1987, till May 15, 1987. Also indicated are the major expendable bathythermograph lines provided by ships of opportunity and two specific tracks where alongtrack analysis is given in Figure 15.

22 passes, each from November 1986 to November 1987 (Figure 1).

As noted in the Geosat geophysical data record handbook [*Cheney et al.*, 1987], wet and dry tropospheric corrections were applied using the Fleet Numerical Oceanographic Center (FNOC) model [*Saastamoinen*, 1972; *Tapley et al.*, 1982]. Ionospheric corrections are based on the global positioning system climatic ionosphere model. Electronic bias was taken into account as 2% of the significant wave height. The tidal signals were removed according to the tide models of *Cartwright and Taylor* [1971] and *Schwiderski* [1980].

The colinear technique was previously tested with success in a mesoscale study of the northwest Atlantic region [*Menard*, 1983]. The analysis includes the following steps: (1) The altimetric measurements of the sea surface are subsampled along each track at 60-km spacing. (2) The mean sea level is then calculated at each point. (3) The differences between each repetitive pass and the mean pass are computed to produce sea level anomalies. (4) The sea level anomalies are adjusted with a second-degree polynomial least squares fit (one degree for short tracks) to absorb the long wavelength errors. A final smoothing is performed using a median filter over 180 km.

This alongtrack analysis is then extrapolated into three dimensional time-space analysis using an objective analysis [*De Mey and Robinson*, 1987]. The objective analysis algorithm was derived from an analytical correlation function described by

$$f = [1 + R(1 + R/3)]^* \exp(-R)^* \exp(-t^2/rct^2)$$

with $R = cste^*r/rcx$, where r is the distance and t is the time separating the interpolated point and any point in the influence radii areas. Based on earlier studies [*Cane*, 1979; *Merle and Arnault*, 1985; *Reverdin and Du Penhoat*, 1987; *Richardson and Reverdin*, 1987] values of 500 km and 140 days were chosen for space and time decorrelation scales rcx and rct. The influence radii that fix the space-time size of the interpolation domain are 300 km and 30 days. The grid size produced is 4° in longitude by 2° in latitude.

One hundred and twenty-five synoptic maps of altimetric sea level anomaly, at 3-day intervals from November 1986 till November 1987, were produced. The error maps calculated by the objective analysis show a mean error of 20 to 25%. Monthly averages of these sea level anomalies were then computed.

2.2. *Climatological Dynamic Height*

The climatological dynamic height relative to 500 dbar was derived from a temperature versus depth profile through a salinity interpolation as described by *Merle and Arnault* [1985]. The data sets contained about 140,000 temperature profiles and 28,000 temperature-salinity (T-S) profiles from 1900 to 1978 and between 16°S, 30°N, the west African coast and 80°W. A large grid spacing, 4° in longitude by 2° in latitude, gives a sufficient number of observations in each box to reduce the confidence interval of the monthly mean temperature to be less than 0.2°C. Annual mean T-S relationships were also computed with the same grid spacing to provide salinity values. Doing this, we have neglected the seasonal variability of the T-S relation. In regions and depths where salinity and temperature vary in phase, like the subsurface central waters, the T-S is not affected by seasonal variation. Near the surface and in regions where the salinity is low and has large variations (e.g., in the northern part of the Gulf of Guinea and in the vicinity of the great rivers (Congo and Amazon)) the T-S relation is affected by seasonal variations. Thus in a given square and for a given month, the total error on the calculated surface dynamic height relative to 500 dbar is the sum for each standard vertical level of the error on the mean temperature and the error due to the neglect of the T-S seasonal variation. We estimated the total error to be less than ±2 dyn cm.

3. Results

3.1. *Comparison of Altimetry with Climatological Dynamic Height*

3.1.1. *Basin-wide study.* A previous study, using historical hydrographic and bathythermal data [*Merle and Arnault*, 1985] analyzed the characteristics of the seasonal signal of the dynamic height (DH) topography in the tropical

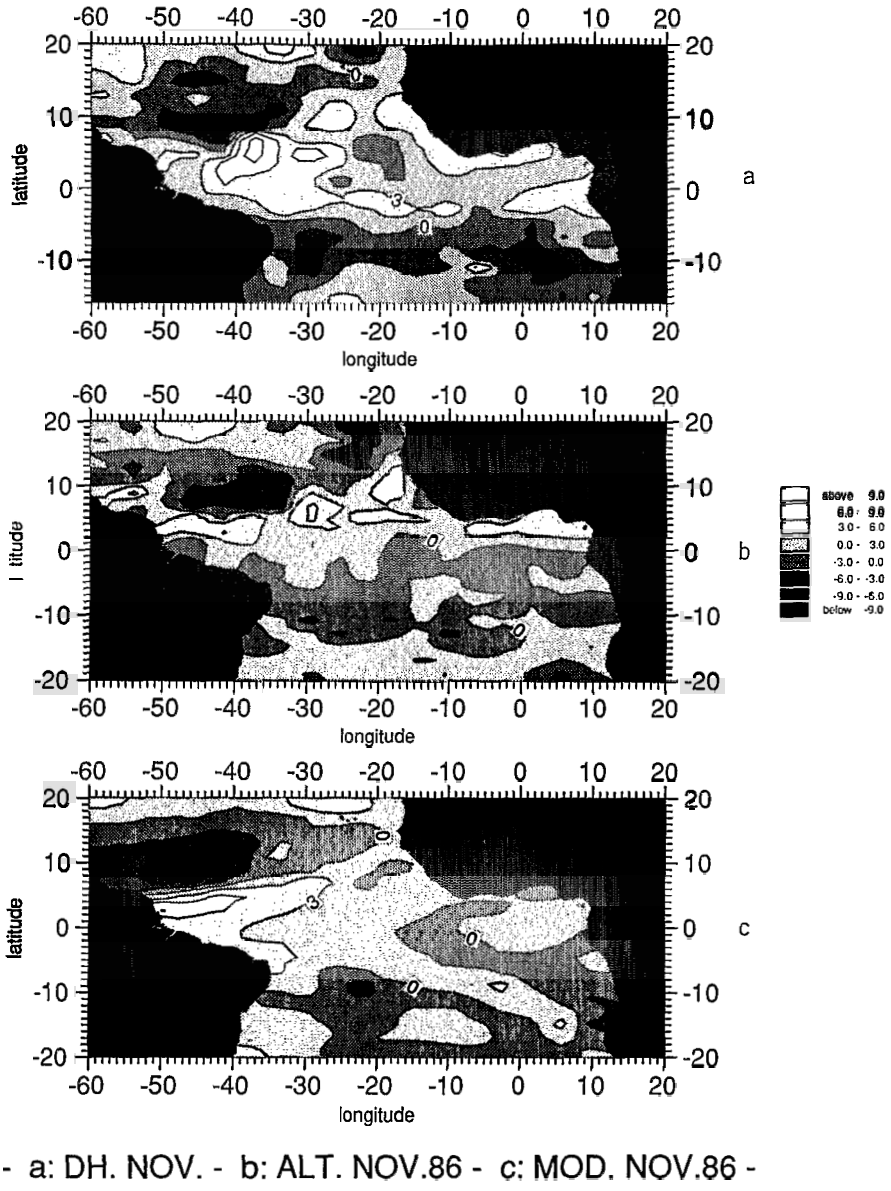

Fig. 2. (*a*) Monthly 0/500 dbar dynamic height anomalies (in dynamic centimeters) for climatological November. (*b*) Monthly altimetric maps for November 1986 (in centimeters). (*c*) Monthly 0/500 dbar dynamic height anomalies (in dynamic centimeters) as computed by the model for November 1986.

Atlantic Ocean. The DH topography in the tropical Atlantic Ocean is the superposition of an east-to-west rise and a series of zonal ridges and troughs. Between the northernmost high at about 15°–20°N and the intermediate low at about 8°–10°N lies the North Equatorial Current (NEC). Further south, at about 2°–3°N, a high borders the southern limit of the North Equatorial Countercurrent (NECC). Close to the equator, but at about 2°–3°S in the Gulf of Guinea, the well-known equatorial low defines the South Equatorial Current (SEC) extending from the northern high (2°–3°N) to a southern high at about 8°–9°S. It is the north equatorial high (2°–5°N) and the equatorial low (0°–3°S) that show the most spectacular month-to-month changes. In this equatorial band, during the winter-spring season (February to June), the DH topography is amorphous in contrast with the summer-fall season (July to November) where the northern high and the equatorial low are well formed.

In order to compare the monthly altimetric anomalies with the DH data, we constructed a set of similar monthly DH anomalies. The monthly DH anomaly maps (Figures 2*a* to 14*a*) show that the seasonal evolution of highs and lows described above results in large and zonal patterns of alternatively positive values (when the DH is higher than the annual mean) and negative values (when it is lower). These positive and negative bands are located on the mean positions of the DH highs and lows mentioned above. These anomalies can fluctuate between 10 and 20 cm, and the stronger signal is observed in the northern hemisphere. The NECC region, between 2° and 8°N, is characterized by positive values from July until January and the SEC region, along the equator, is characterized by negative values during the summer upwelling. This upwelling begins in May near the African coast, and develops toward the center of the basin (30°W) till August. This equatorial upwelling does not

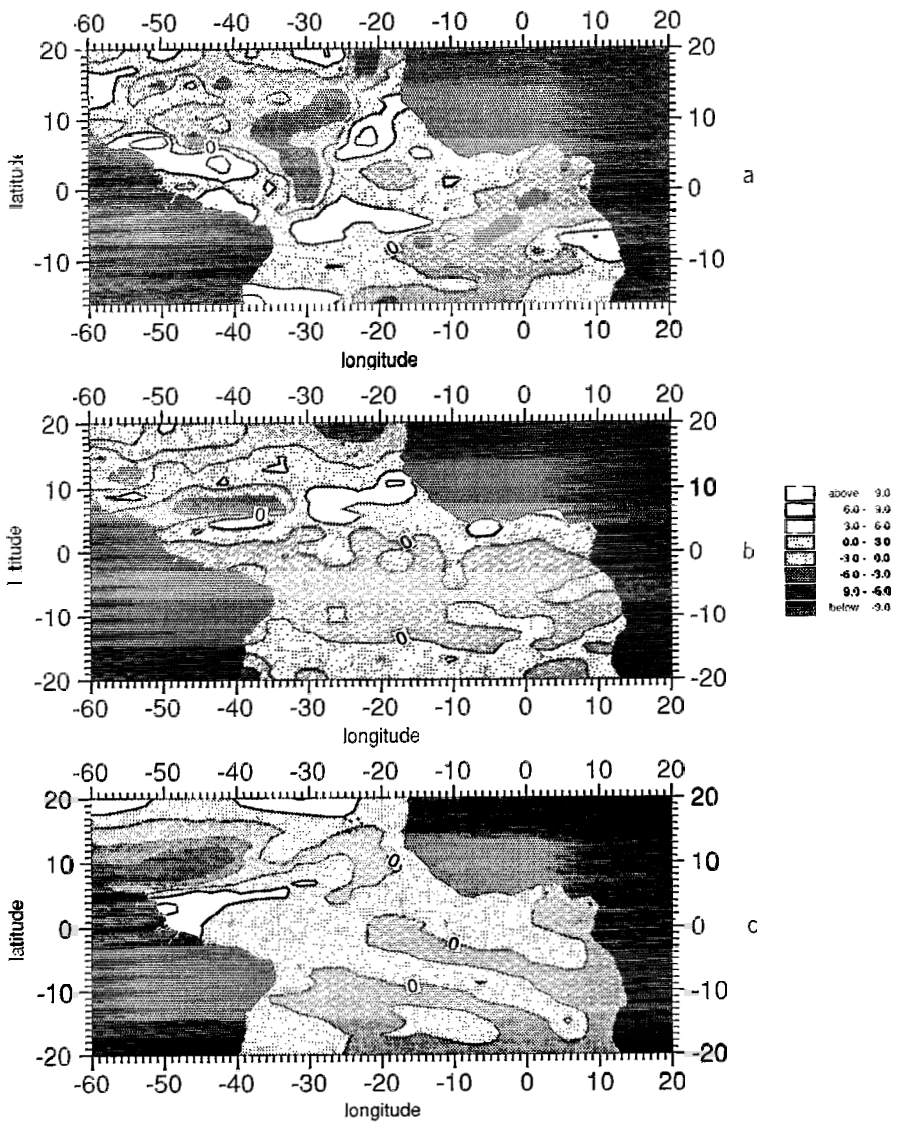

- a: DH. DEC. - b: ALT. DEC.86 - c: MOD. DEC.86 -

Fig. 3. Same as Figure 2 except for climatological December and December 1986.

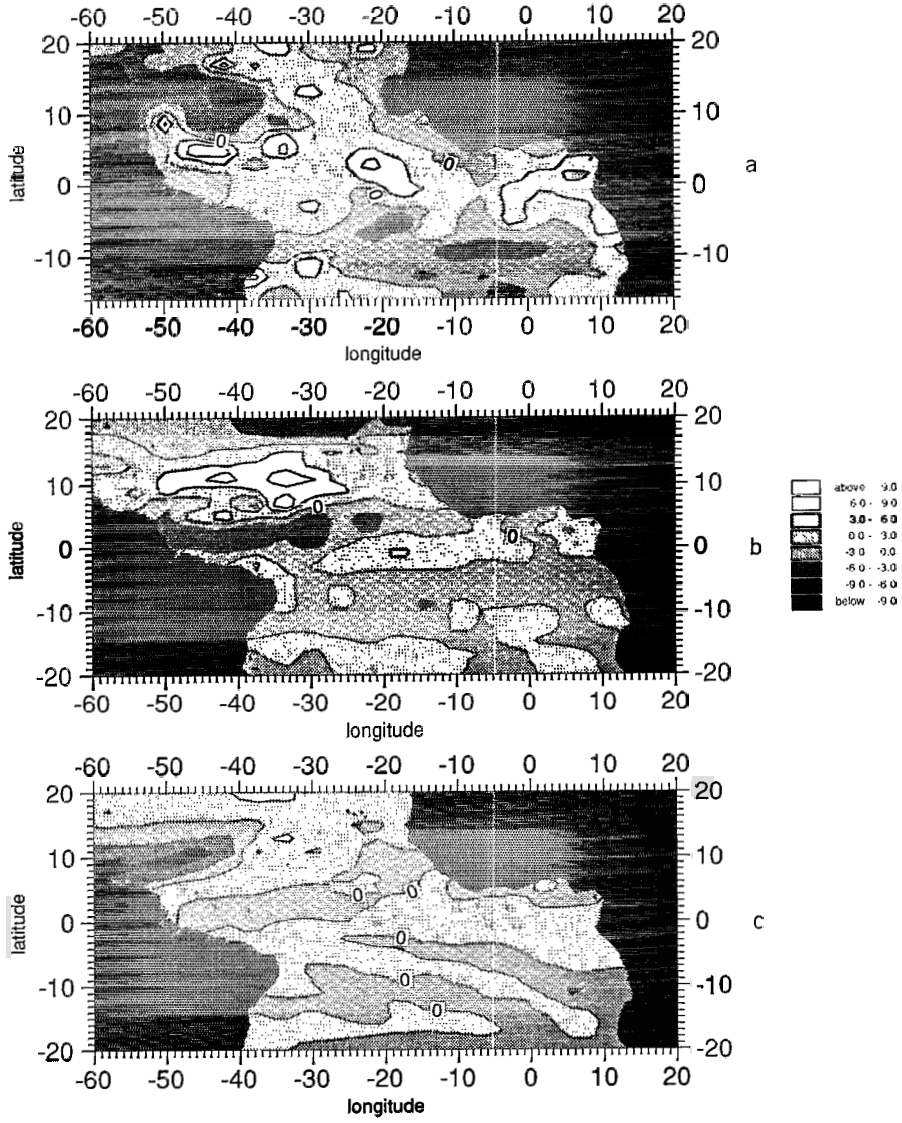

- a: DH. JAN. - b: ALT. JAN.87 - c: MOD. JAN.87 -

Fig. 4. Same as Figure 2 except for climatological January and January 1987.

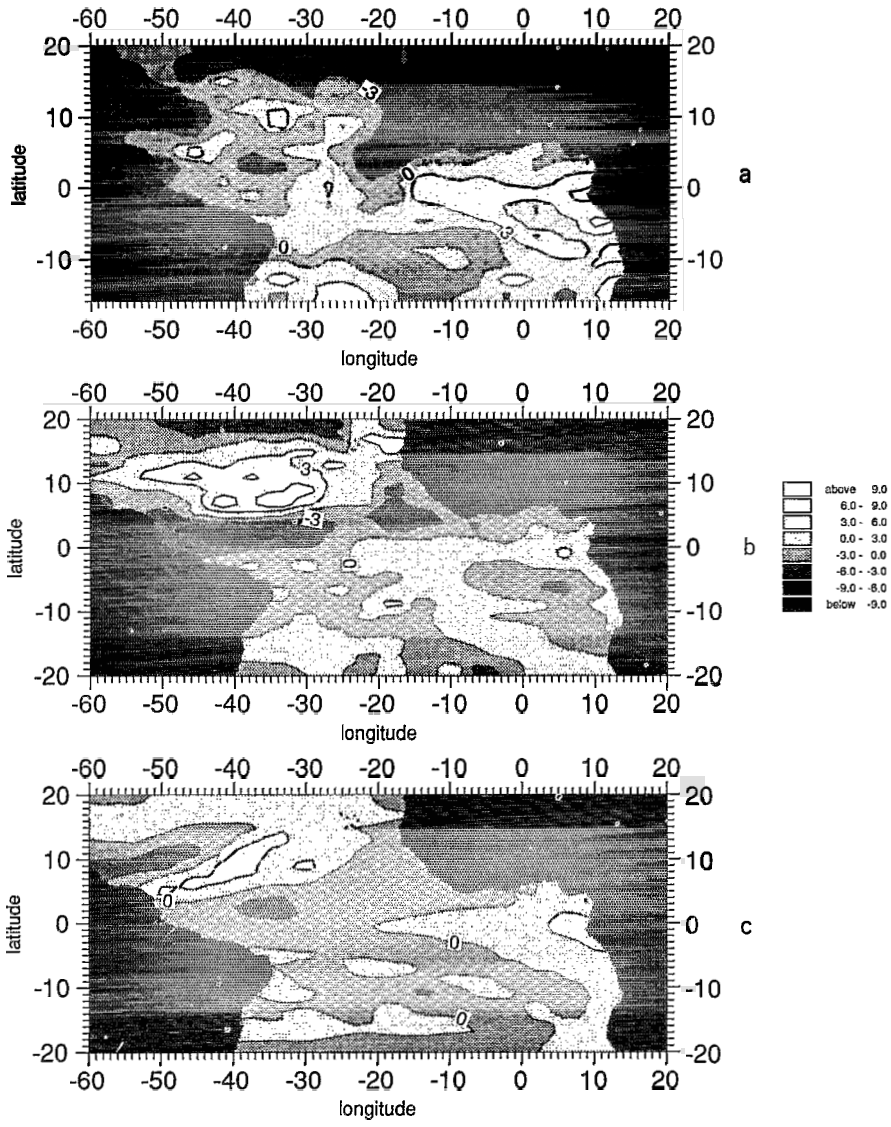

Fig. 5. Same as Figure 2 except for climatological February and February 1987.

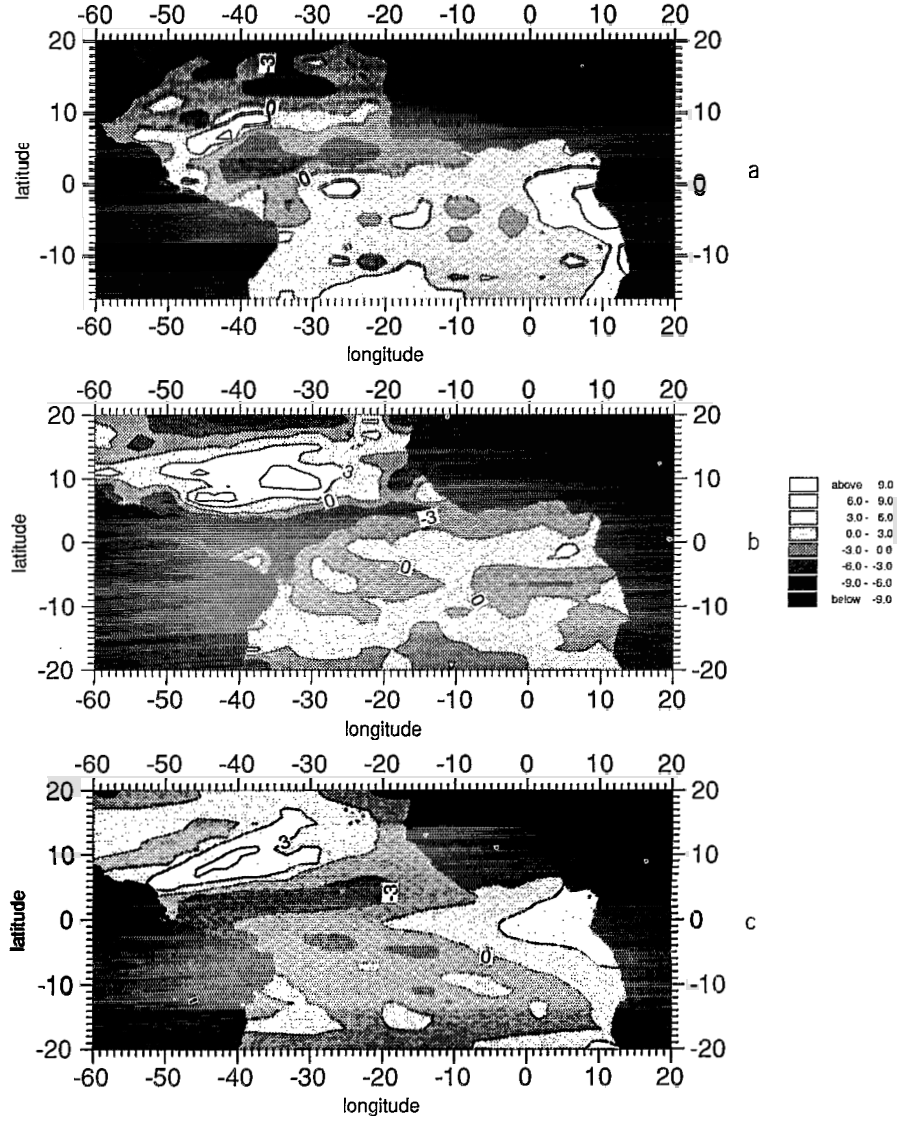

Fig. 6. Same as Figure 2 except for climatological March and March 1987.

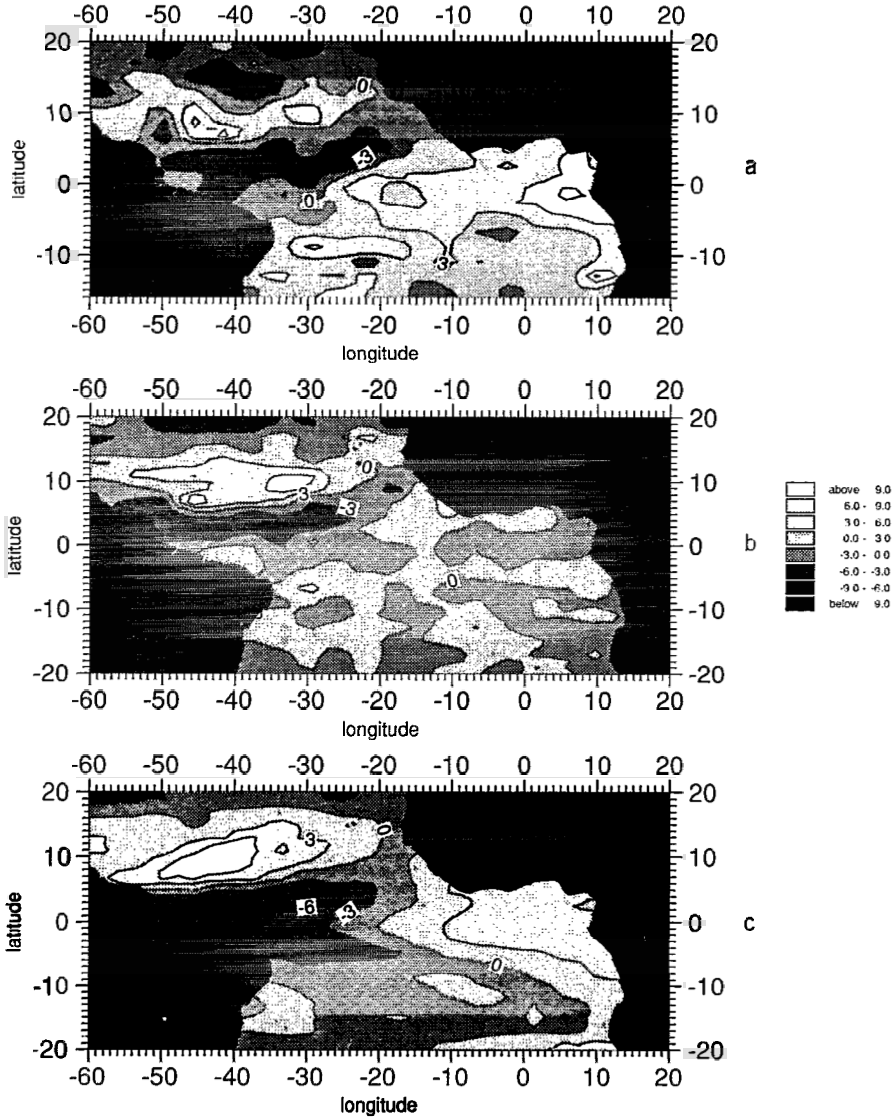

Fig. 7. Same as Figure 2 except for climatological April and April 1987.

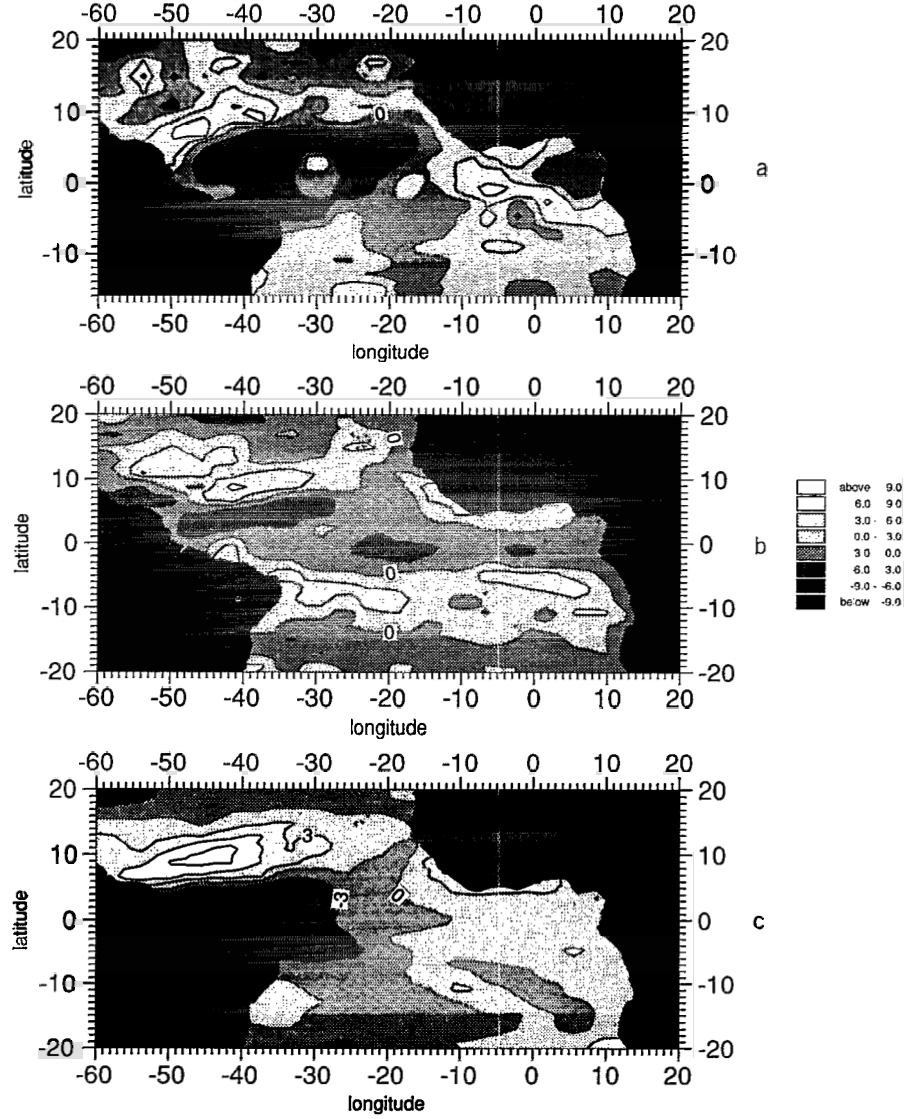

Fig. 8. Same as Figure 2 except for climatological May and May 1987.

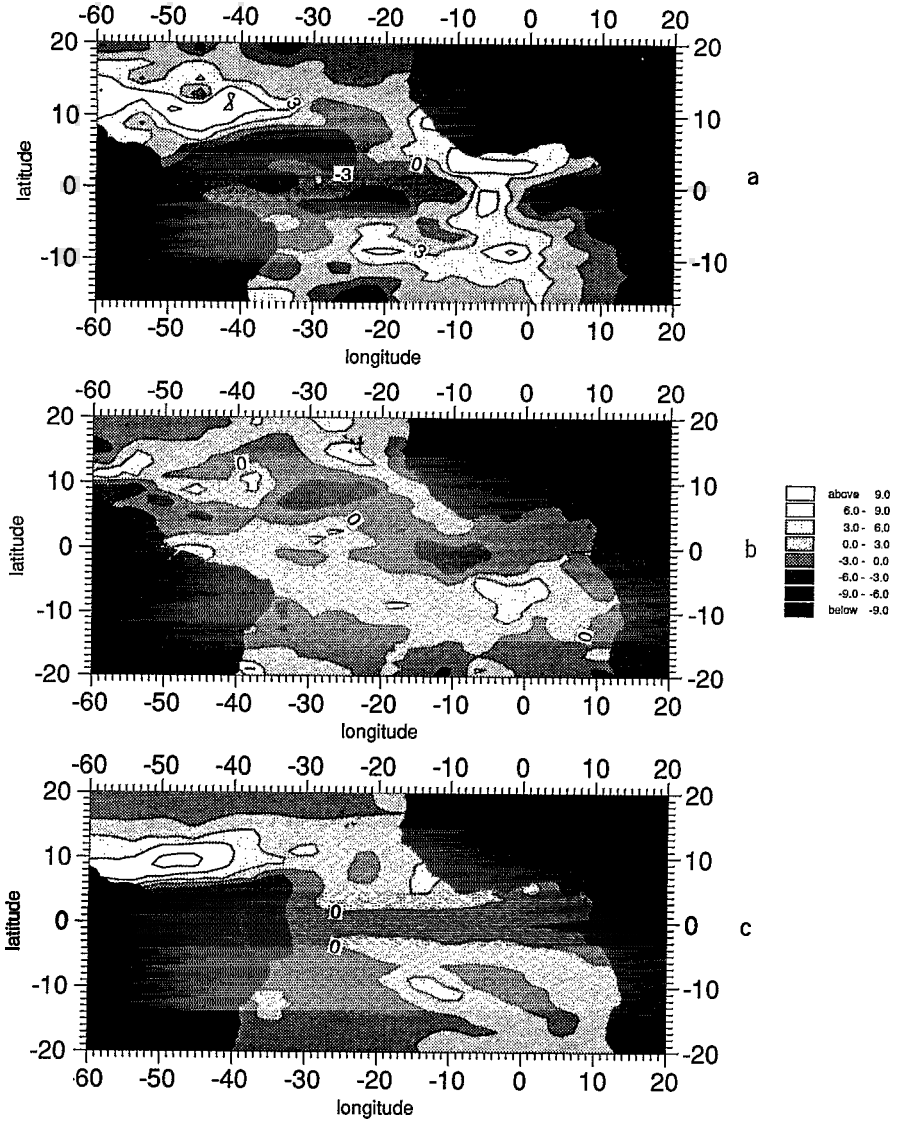

- a: DH. JUN - b: ALT. JUN.87 - c: MOD. JUN.87 -

Fig. 9. Same as Figure 2 except for climatological June and June 1987.

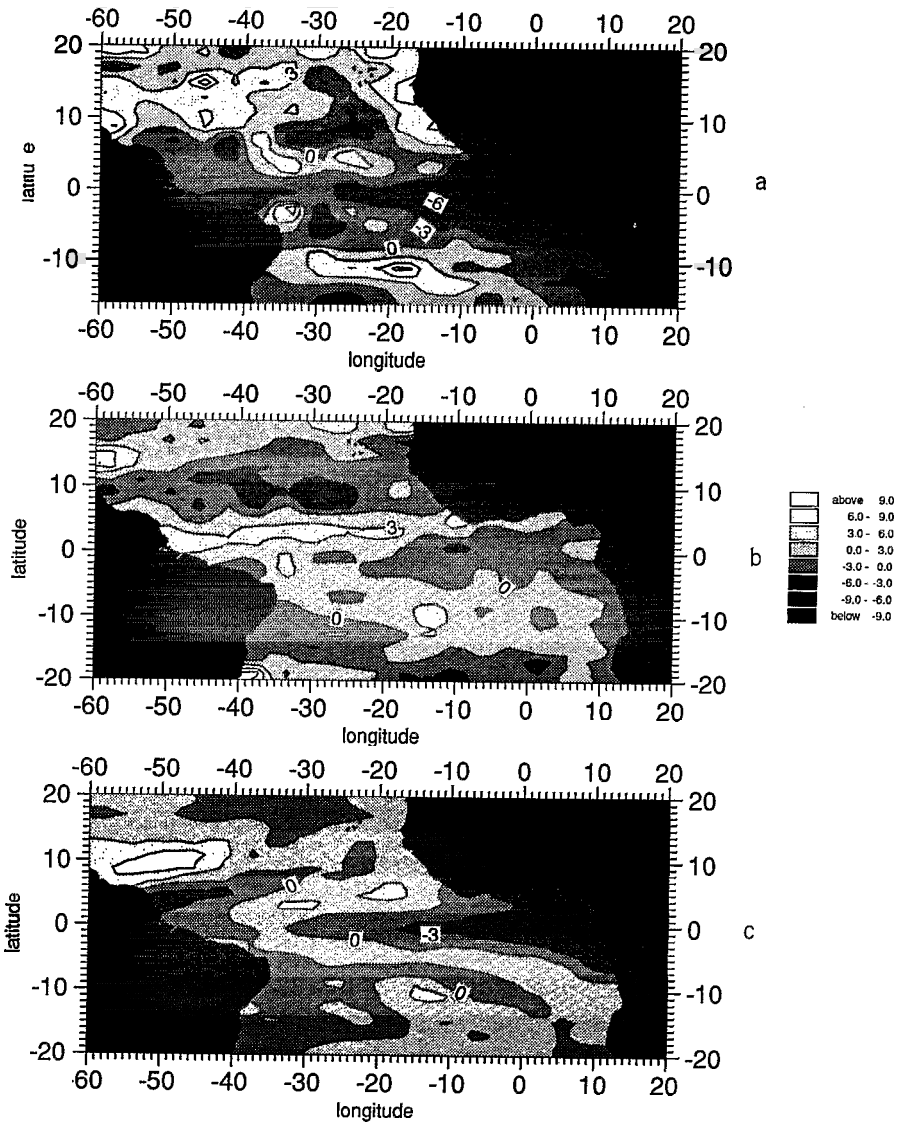

- a: DH. JUL - b: ALT. JUL 87 - c: MOD. JUL 87 -

Fig. 10. Same as Figure 2 except for climatological July and July 1987.

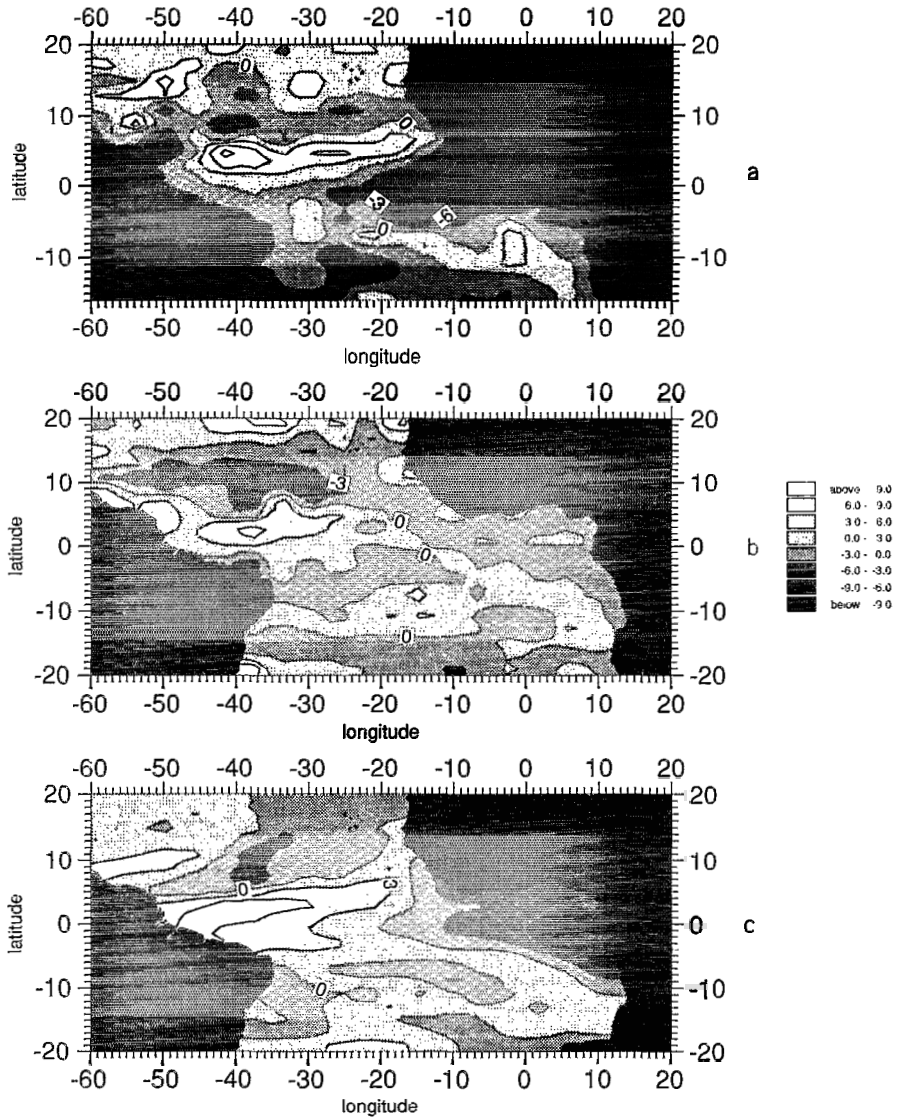

- a: DH. AUG. - b: ALT. AUG.87 - c: MOD. AUG.87 -

Fig. 11. Same as Figure 2 except for climatological August and August 1987.

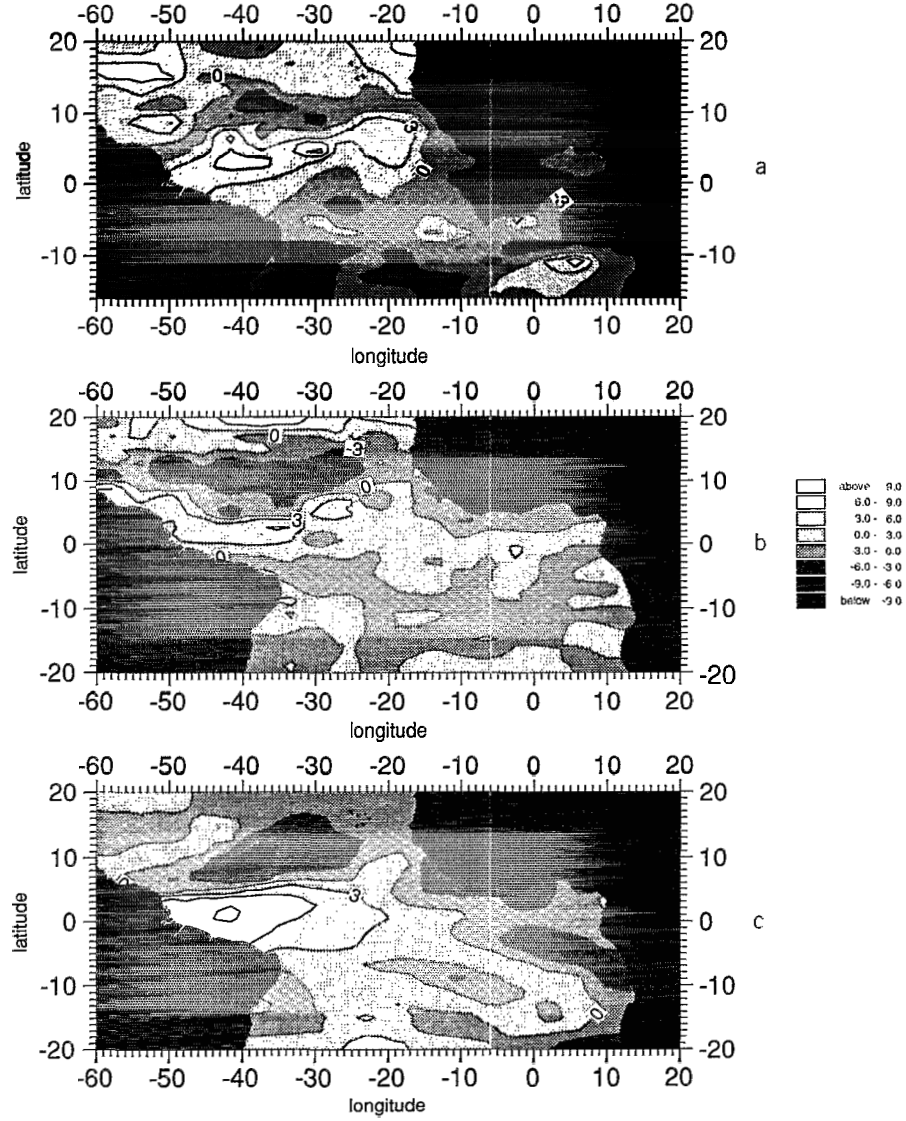

- a: DH. SEP. - b: ALT. SEP.87 - c: MOD. SEP.87 -

Fig. 12. Same as Figure 2 except for climatological September and September 1987.

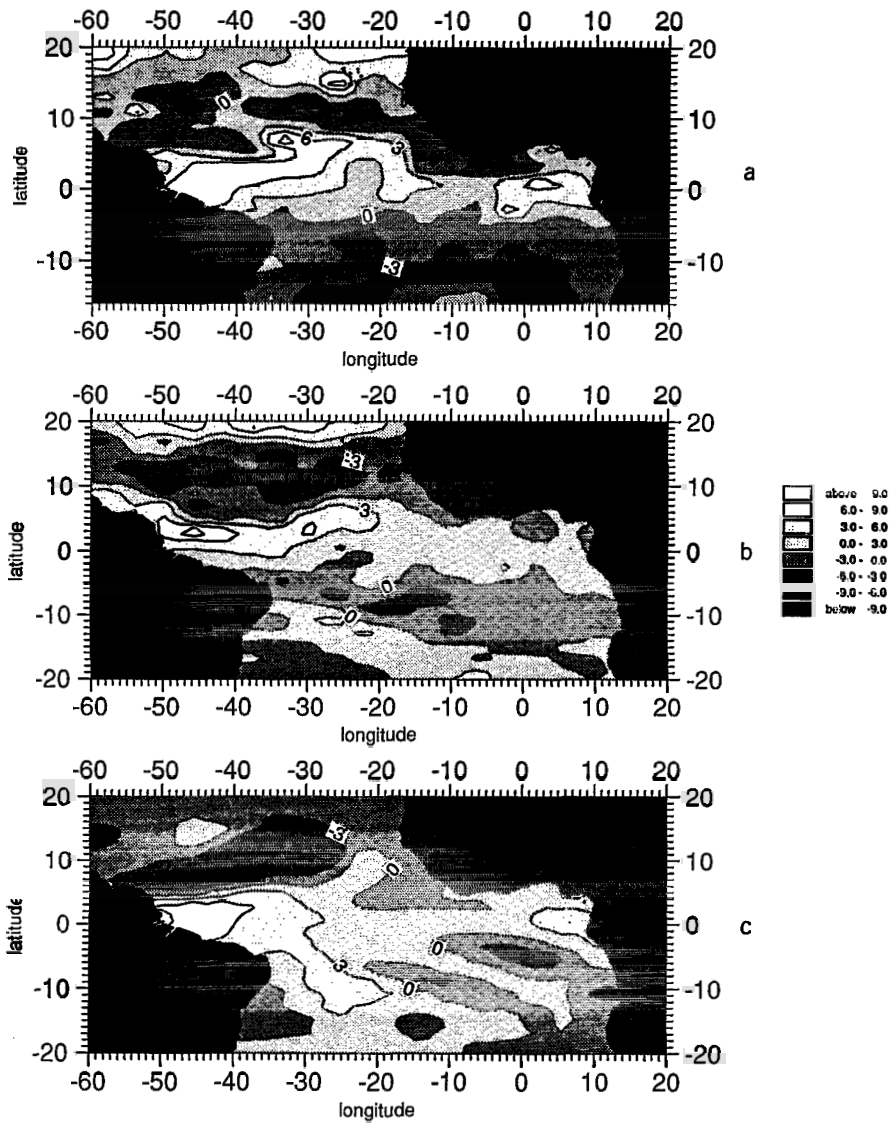

- a: DH. OCT. - b: ALT. OCT.87 - c: MOD. OCT.87 -

Fig. 13. Same as Figure 2 except for climatological October and October 1987.

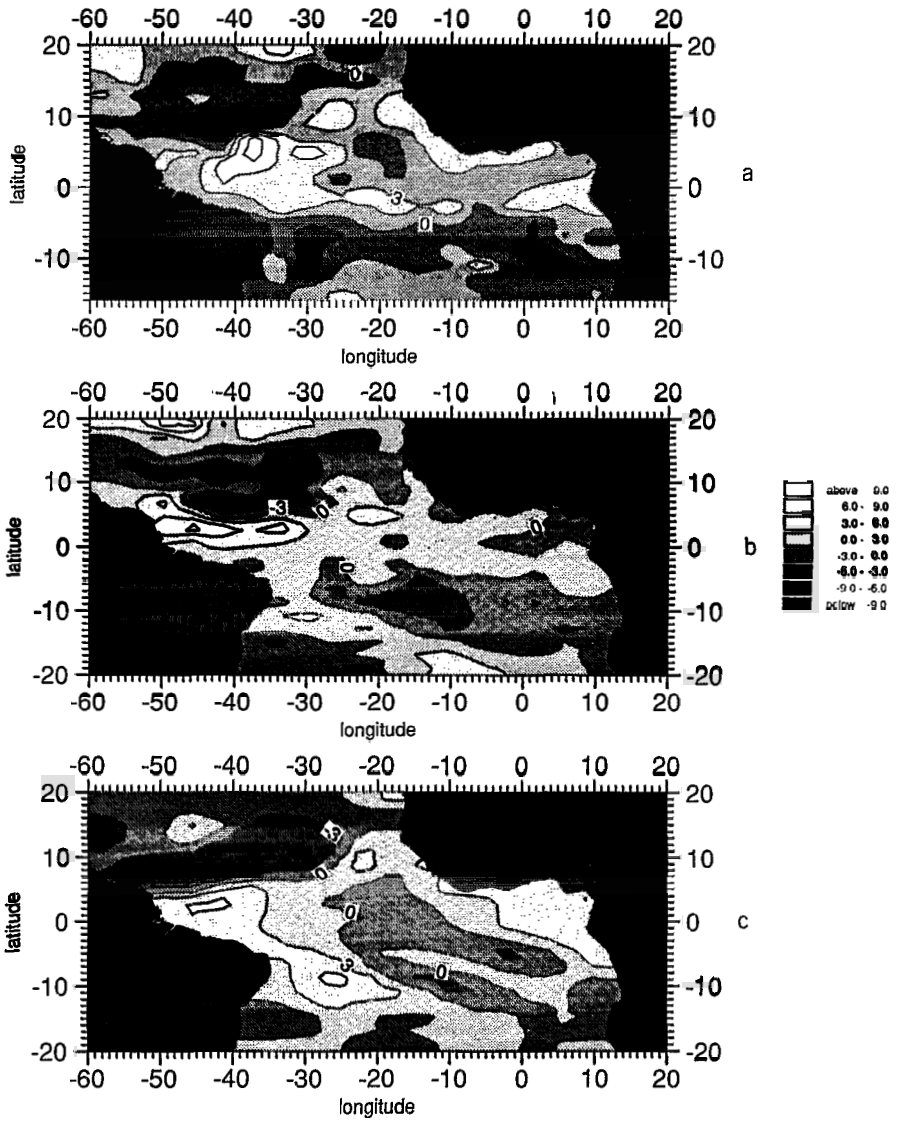

- a: DH. NOV. - b: ALT. NOV.87 - c: MOD. NOV.87 -

Fig. 14. Same as Figure 2 except for climatological November and November 1987.

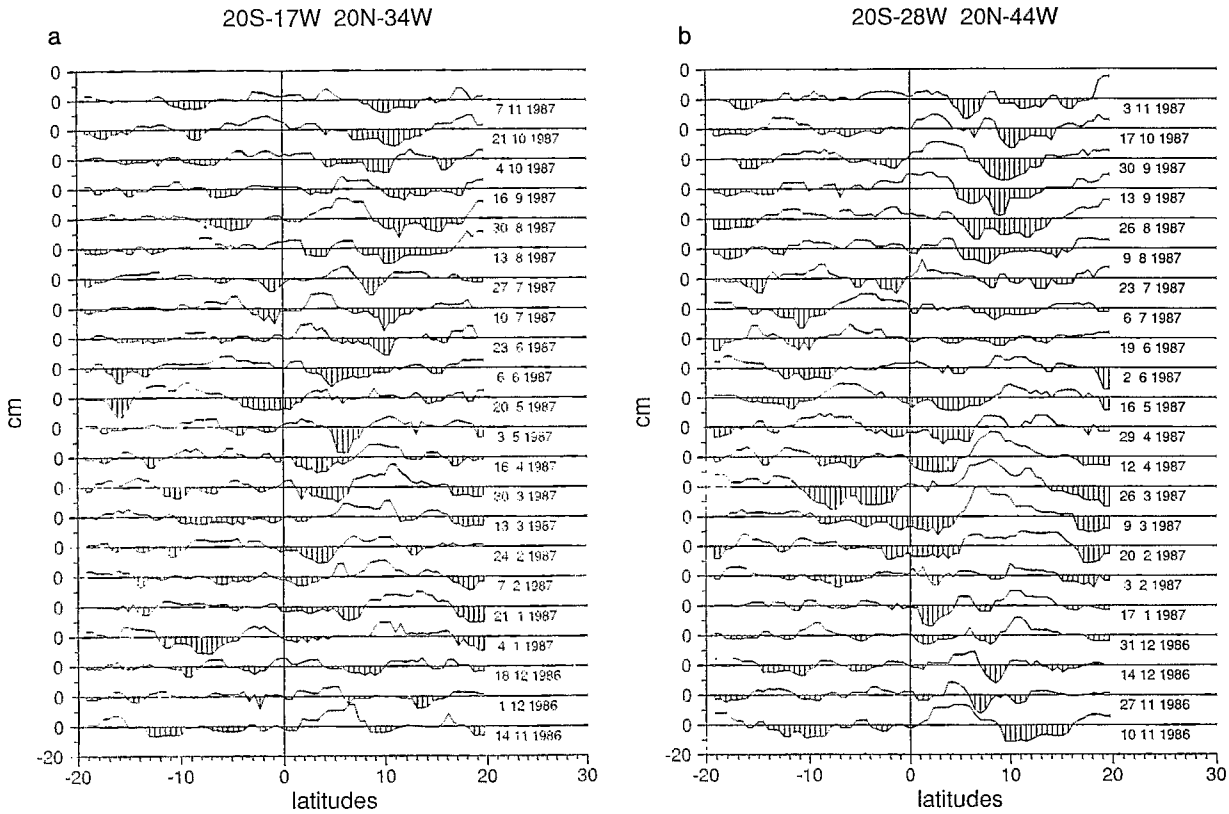

Fig. 15. Alongtrack analysis of altimetric data (in centimeters) from (*a*) 20°S, 17°W to 20°N, 34°W and (*b*) 20°S, 28°W to 20°N, 44°W.

extend as far as 30°W in summer except in July. A secondary cold signal along the equator, in the Gulf of Guinea, is also observed in December when the trade winds strengthen again in the western basin.

The first results obtained from altimetric data, consisting of alongtrack analysis, already agree with this primary description. Figure 15 presents two examples of this alongtrack analysis. One is located in the eastern part of the basin

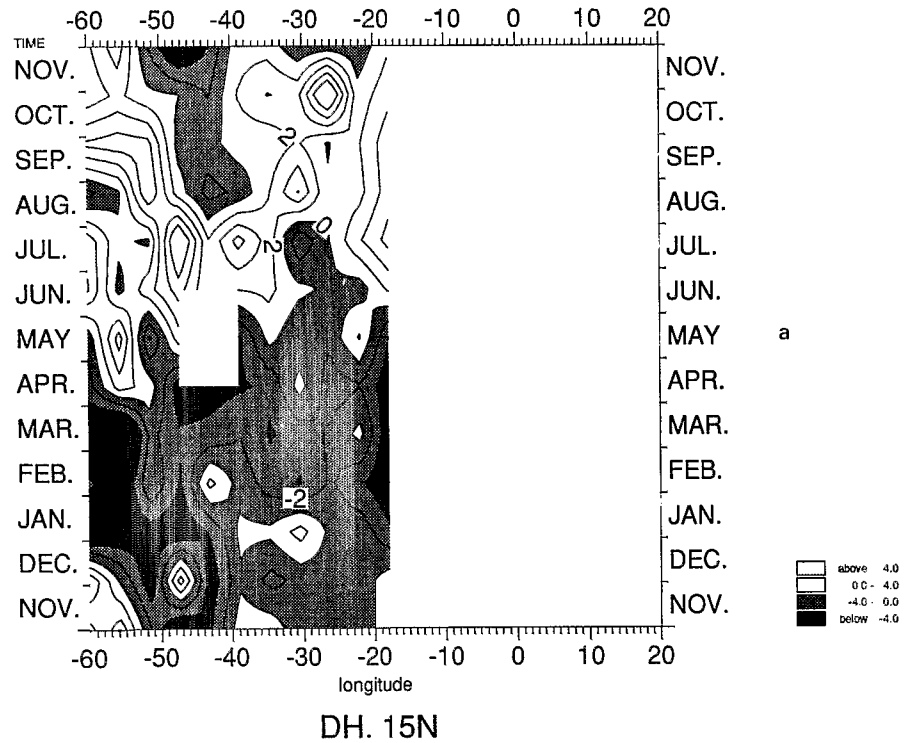

Fig. 16. Time evolution versus longitude in the NEC at 15°N, (*a*) for DH anomalies (in dynamic centimeters), (*b*) for altimetric anomalies (in centimeters), and (*c*) for modeled DH anomalies (in dynamic centimeters).

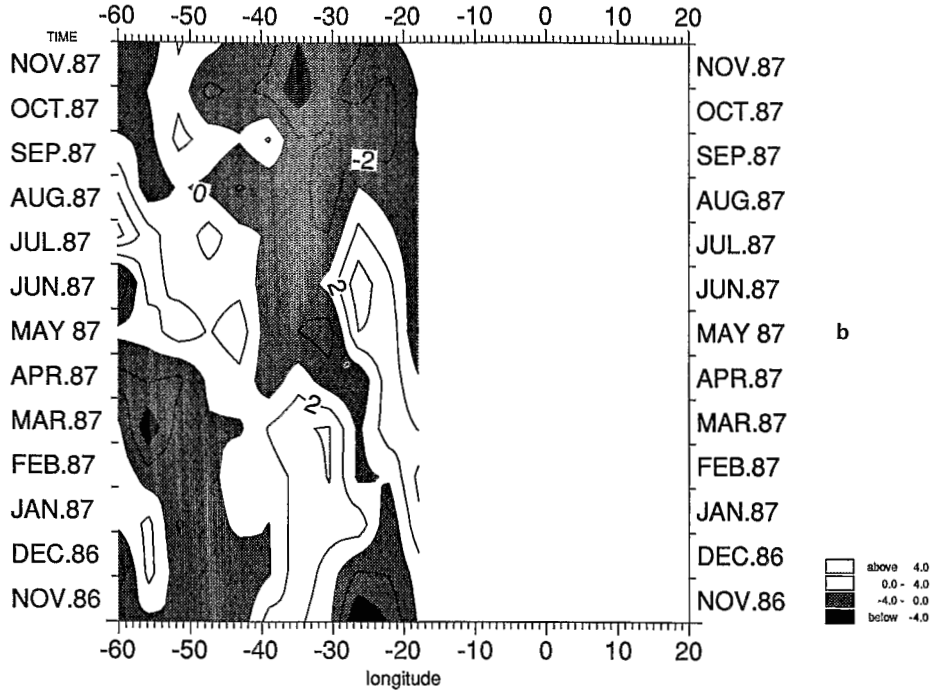

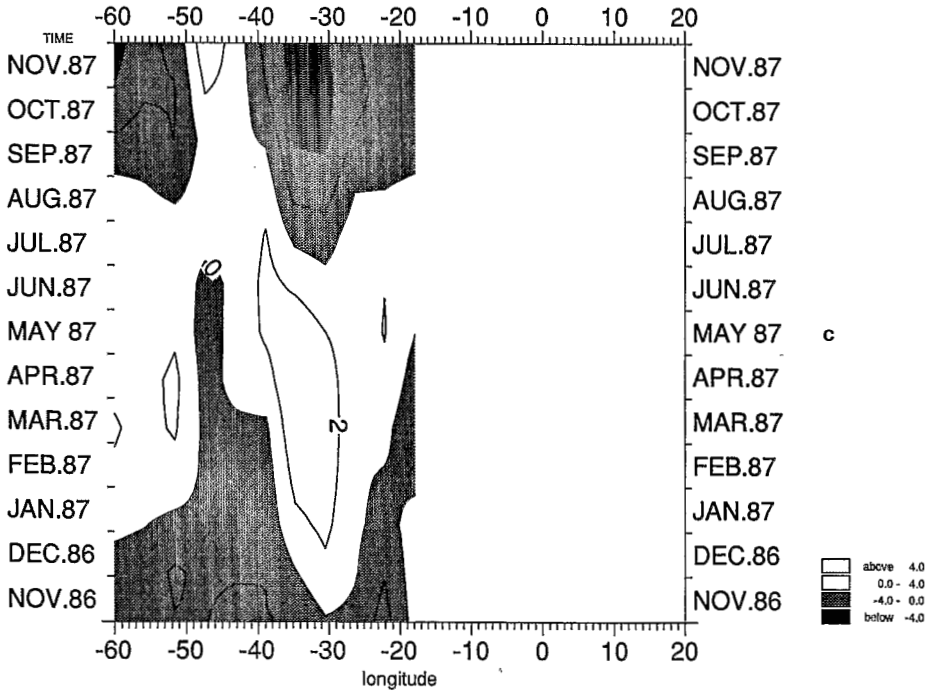

Fig. 16. (continued)

(Figure 15*a*; see Figure 1 for location), the other one is located in the western part (Figure 15*b* and Figure 1). Anomalies of 10–20 cm are clearly identified. As for DH, the signal is stronger in the western part of the basin (Figure 15*b*) than in the eastern part (Figure 15*a*), and in both cases, peaks and troughs are more developed in the northern hemisphere. Along the equator, a negative anomaly develops by the beginning of May 1987 and lasts over the 1987 summer season in the eastern track. The western track, crossing the equator at 36°W, shows a weaker or even nonexistent signal, in agreement with the climatological DH. This western track also presents a NECC high rising around

TABLE 1. Root-Mean-Square Differences Between Climatological 0/500 dbar Dynamic Height and Altimetric Anomalies as a Function of Time and Geographic Area

	N86	D86	J87	F87	M87	A87	M87	J87	J87	A87	S87	O87	N87
World ocean	2.6	3.0	3.6	3.5	3.6	3.3	3.1	3.9	4.1	3.9	3.5	3.0	2.8
NEC (12–18°N)	2.7	3.2	2.9	2.5	2.7	2.4	2.1	2.9	3.0	2.6	3.2	2.5	2.7
NECC (4–8°N)	1.7	2.8	2.6	2.8	2.4	2.1	3.1	2.5	2.1	3.1	2.4	1.5	1.9
SEC (0–2°N)	1.3	2.4	1.7	2.0	2.5	5.0	4.5	3.6	1.9	3.0	2.7	1.7	1.8
SEC (2–8°S)	2.5	3.3	2.9	3.0	3.4	3.0	3.6	4.7	3.2	4.2	3.4	3.0	3.3

Read N86 as November 1986. Values are in centimeters.

3°N by the end of June to reach more than 10 cm in late September.

The rough agreement between DH and altimetric anomalies is even more evident in monthly altimetric anomaly maps obtained from this alongtrack analysis through an objective analysis. If we compare the monthly DH anomaly maps (Figures 2*a* to 14*a*) with monthly altimetric anomaly maps (Figures 2*b* to 14*b*), they present the same succession of positive and negative anomalies but with altimetric values generally lower by 2–3 cm than the DH. In the western part of the basin, the meridional tilting along the mean position of the intertropical convergence zone (ITCZ), which has been observed using different in situ data sets [*Merle*, 1983; *Garzoli and Katz*, 1983], is well described by altimetry. The upwelling signal along the equator is starting from the African coast but in April 1987 instead of May in the DH climatology. A very slight secondary upwelling seems to occur in January 1987 in the Gulf of Guinea that corresponds to the secondary cold season observed by many authors in the Gulf of Guinea [*Merle et al.*, 1979]. Mean rms differences between altimetry and DH all over the basin vary from 2.6 cm in November 1986 to 4.1 cm in July 1987 (Table 1). As we will see later, this worse agreement in summer is due mainly to the equatorial and south equatorial upwellings.

3.1.2. *Regional study.* This first global comparison between climatological DH and altimetry has revealed that for a basin-wide scale, both types of data present the same structures with some little discrepancies. In order to evidence how these differences between the two data sets are dependent on geographic locations, we have divided the basin into zonal bands located on the mean positions of the major currents in the tropical Atlantic Ocean.

The NEC region (12°–18°N): The rms difference between altimetry and DH anomalies in the NEC region is around 2–3 cm (Table 1). Time series versus longitude at 15°N are given in Figure 16 for altimetric and DH anomalies. The altimetric data (Figure 16*b*) show out-of-phase signals apart from 40°W. West of 40°W, the signal is mostly positive during boreal summer (May 1987 to October–November 1987) and negative during winter. East of 40°W, altimetry presents a totally opposite signal with negative values in summer–fall 87 and positive values in winter.

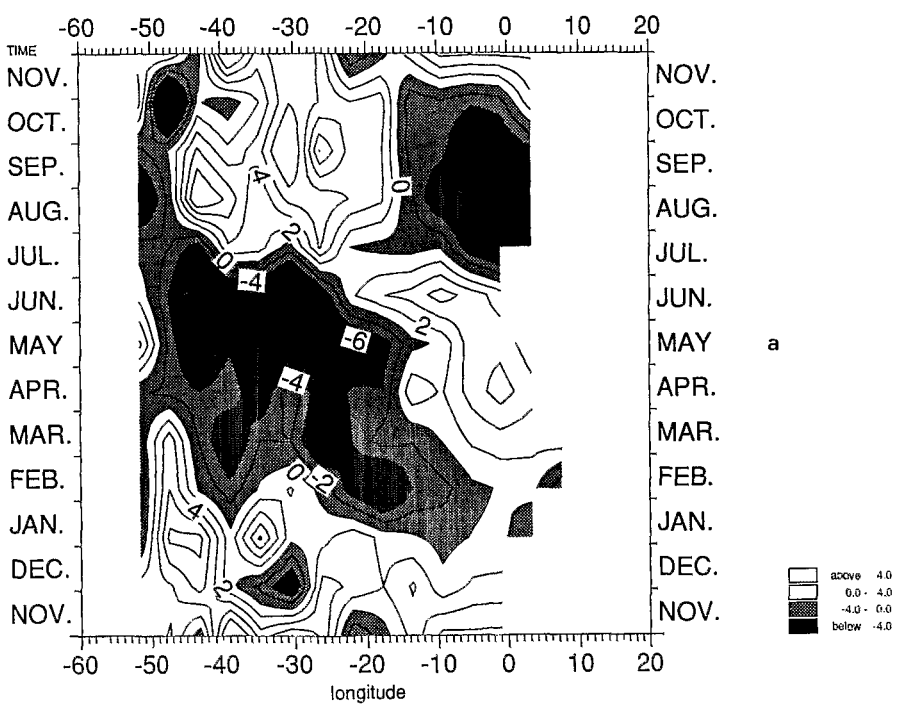

DH. 5N

Fig. 17. Same as Figure 16 in the NECC at 5°N.

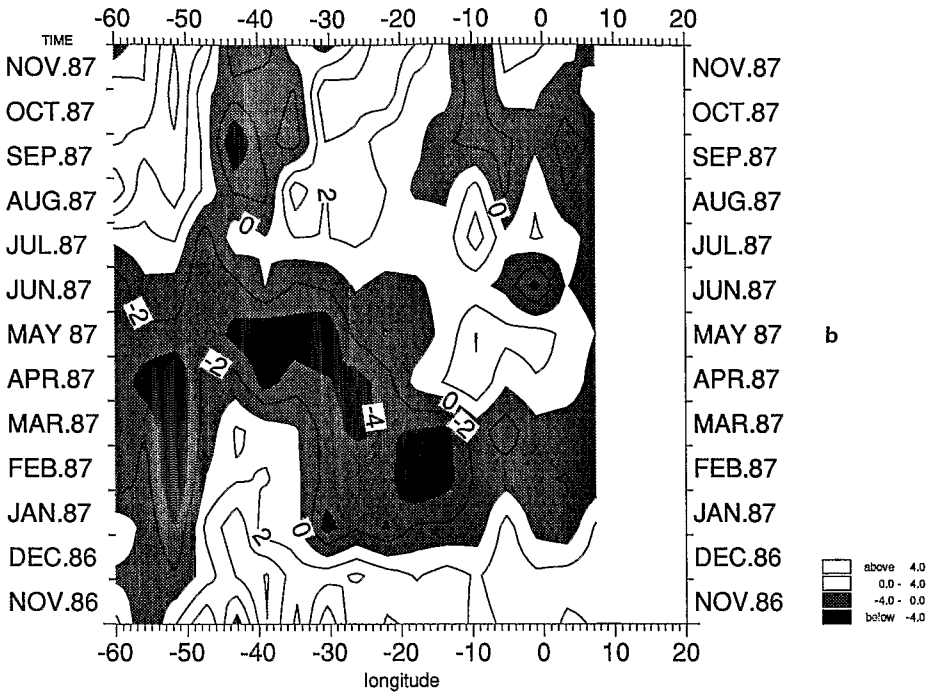

ALT. 5N

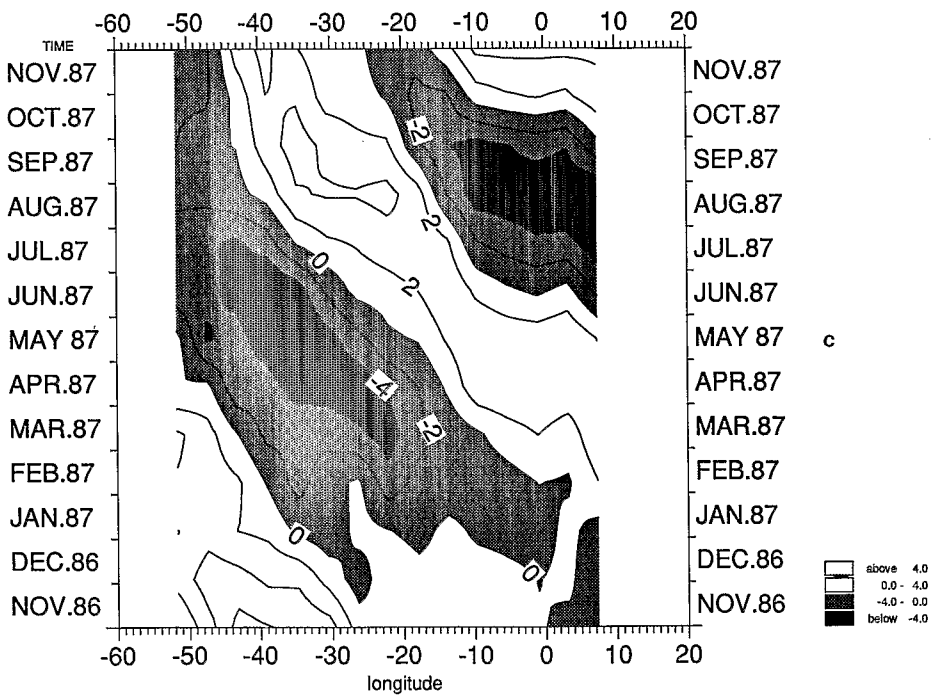

MODEL 5N

Fig. 17. (continued)

West of 40°W, the DH signal (Figure 16*a*) is identical to the altimetric one, but altimetric values are lower than climatology: 4 cm for the maxima instead of 6–8 cm. East of 40°W, in reverse, the two signals are different and even more out of phase.

The NECC region (4°–8°N): The mean rms difference between altimetry and DH anomalies between 4° and 8°N is less than 3 cm (Table 1). The agreement between altimetry and DH is particularly good in October–November when the NECC is fully developed [*Richardson and McKee*, 1984;

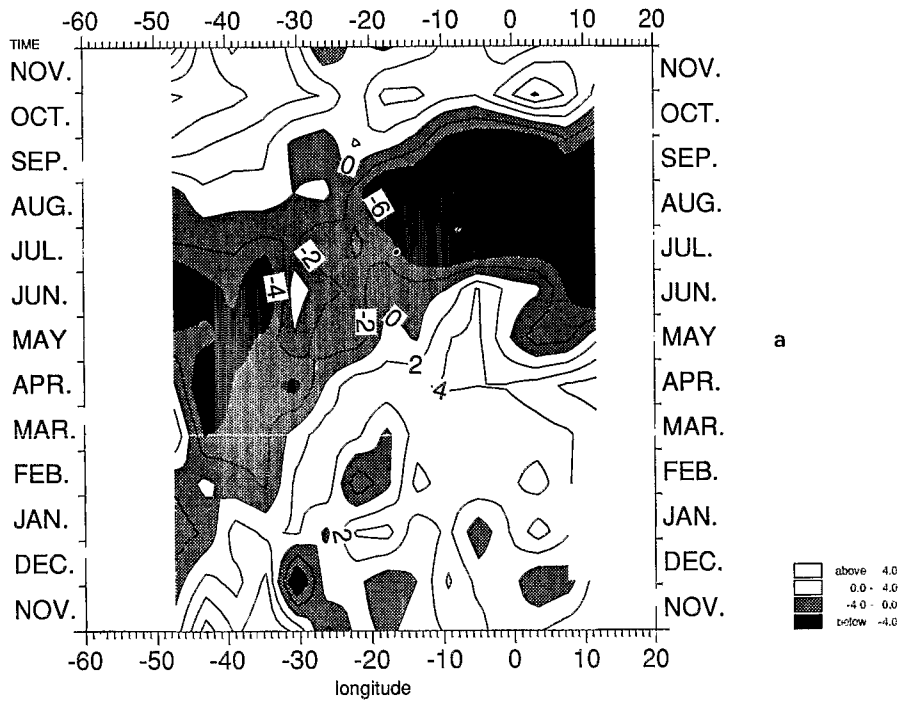

Fig. 18. Same as Figure 16 in the SEC at 1°N.

Arnault, 1987]. The altimetric signal at 5°N (Figure 17*b*) presents positive anomalies in November–December 1986 as far as 50°W. Then negative values occur, starting in January 1987 at 10°W, ending in June–July 1987 in the west. When the northern high is developing, in April–May 1987 near the African coast until late autumn near the Brazilian coast, positive values appear again.

At 5°N the DH evolution is very similar to the altimetric one (Figure 17*a*) but altimetric values are lower again especially during summer–fall 1987: 4 cm instead of 8 cm. It is interesting to note that the semiannual signal which appears in DH east of 20°W is also present in altimetry.

The SEC region (2°N to 8°S). As was seen previously, this region is affected by the largest differences between altimetry and DH. In boreal summer, during the equatorial upwelling, the rms difference can reach more than 4 cm south of the equator (Table 1). The time-longitude evolution of altimetric data at 1°N (Figure 18*b*) shows two distinct regions apart from 25°W. East of 25°W, in the Gulf of Guinea, the signal is characterized by a slight negative extremum in November–December 1986, when the westward equatorial winds reintensify, followed by another, larger one in spring–summer 1987. West of 25°W, we find an annual signal with negative anomalies starting from December 1986 to January 1987 and ending in May 1987.

Comparison with DH also at 1°N (Figure 18*a*) shows that if the time evolutions are very similar with the same division of the basin into eastern semiannual and western annual signals, the altimetric amplitude is lower again, especially in the east (−2 cm instead of −8 cm), and above all, there is an important time shifting between altimetry and DH. Near the African coast, the beginning of the equatorial upwelling which occurs in March–April 1987 for altimetry, is shifted to May–June in DH.

The pattern at 1°S (Figure 19) is very similar to what has been observed at 1°N, with the same time shifting of the equatorial upwelling in the altimetric data. It will be discussed further whether these discrepancies are due to some altimetric data artifact or to interannual variability.

3.1.3. *Seasonal variability.* As was noticed earlier, the maximum variability occurs in the northern hemisphere, in the western part of the basin. Altimetric data (Figure 20*b*) show a maximal seasonal variability (more than 8 cm) between 25° and 45°W, extending from 3°N in the west to 10°N in the east. Along the coasts in the Gulf of Guinea, a second maximum (4 cm) appears. Lower values (2 cm) separate these two altimetric variability extrema.

DH seasonal variability (Figure 20*a*) also reaches more than 7 cm between 25° and 45°W. A second maximum is found along the equator in the east, with a net south shifting near the African coast where the amplitude reaches more than 6 cm. Between these two extrema, a zone of lower variability extends. What is very intriguing is the lack of variability found for the altimetric signal in the Gulf of Guinea when compared with the large seasonal variability found in the DH data. This has already been observed by *Menard* [1988] using GEOS 3 and Seasat altimeters.

3.2. *Comparison of Altimetry With 1986–1987 in Situ Data*

As was mentioned above, climatology of the DH neglects interannual variability. A large part of the discrepancies found between altimetric data and DH data could be due to

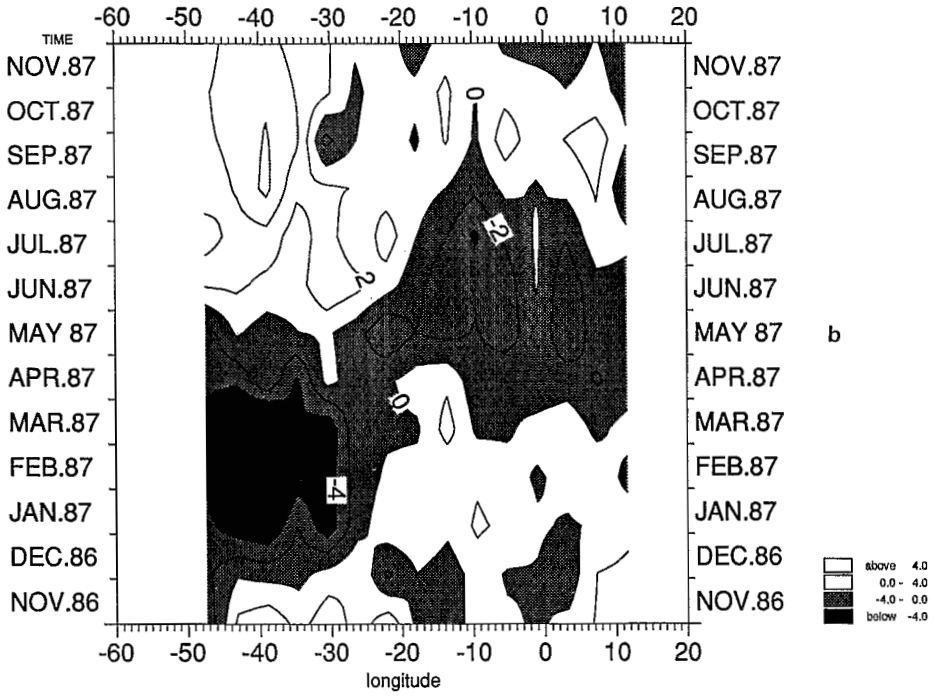

ALT. 1N

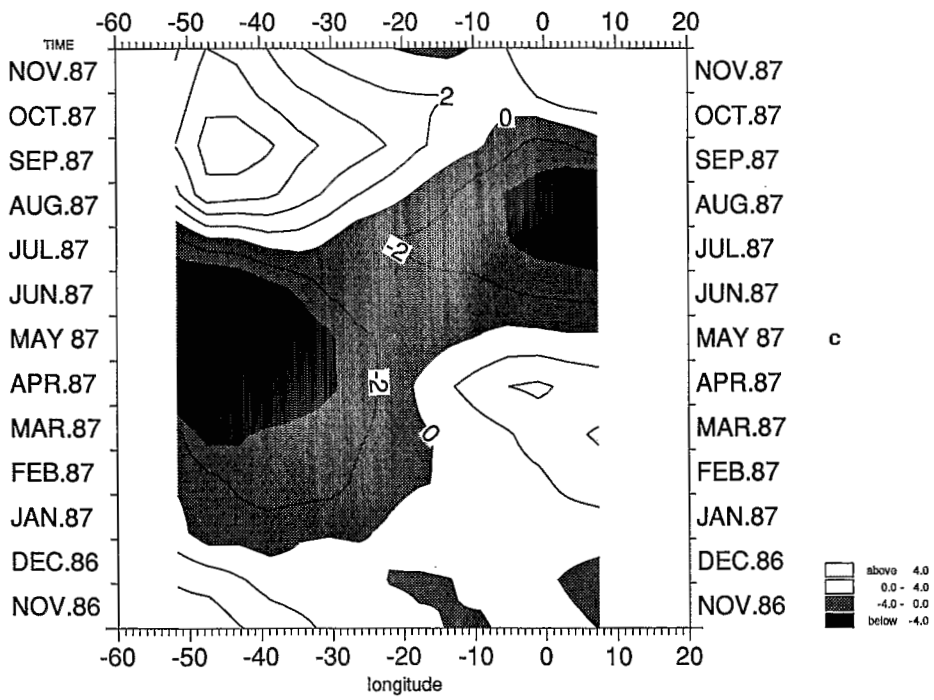

MODEL 1N

Fig. 18. (continued)

the fact that the 1986–1987 year is abnormal compared with the climatology. Comparing the 1986–1987 altimetric data with 1986–1987 in situ data would shed some light on these uncertainties. Unfortunately, this year is rather poor in observations, unlike the 1982–1984 FOCAL/SEQUAL period. Nevertheless, we have IES records (courtesy of E. Katz) and Tropical Ocean–Global Atmosphere (TOGA) expendable bathythermograph (XBT) lines converted to DH by G. Reverdin (personal communication, 1988).

E. Katz kindly provided us the records of five IES located

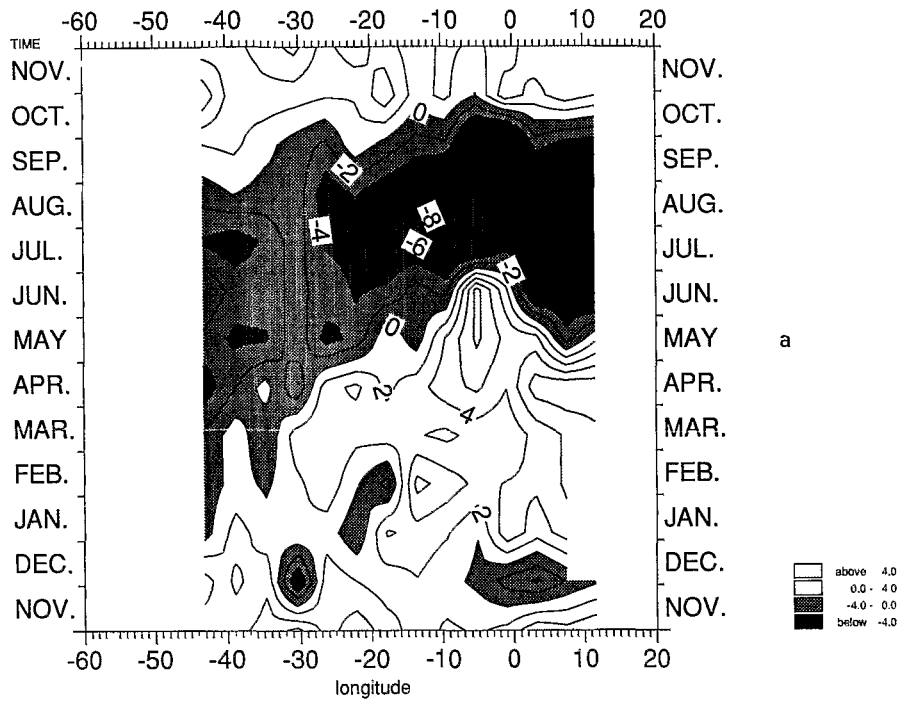

Fig. 19. Same as Figure 16 in the SEC at 1°S.

at 9°N, 38°W; 3°N, 38°W; 0°, 38°W; 7°N, 44°W; and 3°N, 44°W. The raw IES data were processed as described by *Katz* [1986] to obtain the DH anomaly: first, the tidal signal was removed using a tide filter, then a low-pass filter at 10 days was applied, and finally IES data were converted to DH anomalies. We have compared these IES/DH signals to those given by altimetry in the surrounded square. At 3°N, near the southern border of the NECC, the two sets of data are highly correlated (Table 2 and Figures 21*b* and 21*e*): the correlation coefficients are 0.94 at 38°W and 0.82 at 44°W, so that more than 67% of the IES signal is explained by altimetry. Along the equator (Figure 21*c*), the correlation is slightly weaker: around 0.7, which is rather good for an area of high stratification where usually the IES data are more difficult to relate to DH. More surprising are the results at 7°N and 9°N (Figures 21*a* and 21*d*), where the correlations are rather bad: 0.36 and 0.55, but the IES data appear more noisy and could not correctly reflect the DH. Moreover, in this region, large moisture effects can generate in the Geosat data errors of a few centimeters not necessarily well corrected by the FNOC model. This was emphasized in several studies showing comparisons between various tropospheric correction models [*Monaldo*, 1990; *Jourdan et al.*, this issue]. In the future, new special sensor microwave imager (SSM/I) based corrections will allow a more effective reduction of these error sources [*Emery*, 1990].

The other set of 1986–1987 data was provided by G. Reverdin (personal communication, 1988). He computed DH using mean *T-S* profiles and expendable bathythermographs (XBT) launched by ships of opportunity in the tropical Atlantic. There are two lines of merchant ships which cross the tropical Atlantic Ocean. The first one is from Dakar to Rio de Janeiro/Buenos Aires, the other one is from the Antilles to South Africa (see Figure 1 for location). The XBTs were averaged by 1.5° latitude boxes. The evolution of the DH and altimetric anomalies from November 1986 until November 1987 along these lines between 5°N and 5°S is given in Figure 22. The agreement between the two data sets is reasonably good, especially at 4.5°N, 3°N, 1.5°N, 1.5°S, and 3°S for the western line and at 3°N and 1.5°S for the eastern line. Along the equator, altimetry and DH vary in phase in the west and in the east, at 1.5°S.

Then it seems that most of the time shifting in the seasonal upwelling signal between the climatology and the altimetric data in 1987 is due to the interannual variability. The year 1987 seems to be characterized by an earlier summer upwelling. This point will be confirmed later with the model simulation.

4. Comparison of Altimetric Data With A Numerical Simulation

4.1. *Description of the Model*

The model we used computes the linear response of the tropical Atlantic Ocean to the wind forcing through three baroclinic modes. *Du Penhoat and Treguier* [1985] have shown that 95% of the signal obtained with nine modes is provided by the first three. More recently, *Du Penhoat and Gouriou* [1987] demonstrated the ability for this kind of model to reproduce DH topography interannual events, and at a much lower cost than three-dimensional primitive equation models. They captured quite well the 1983–1984 contrast in the tropical Atlantic Ocean which was the result of an

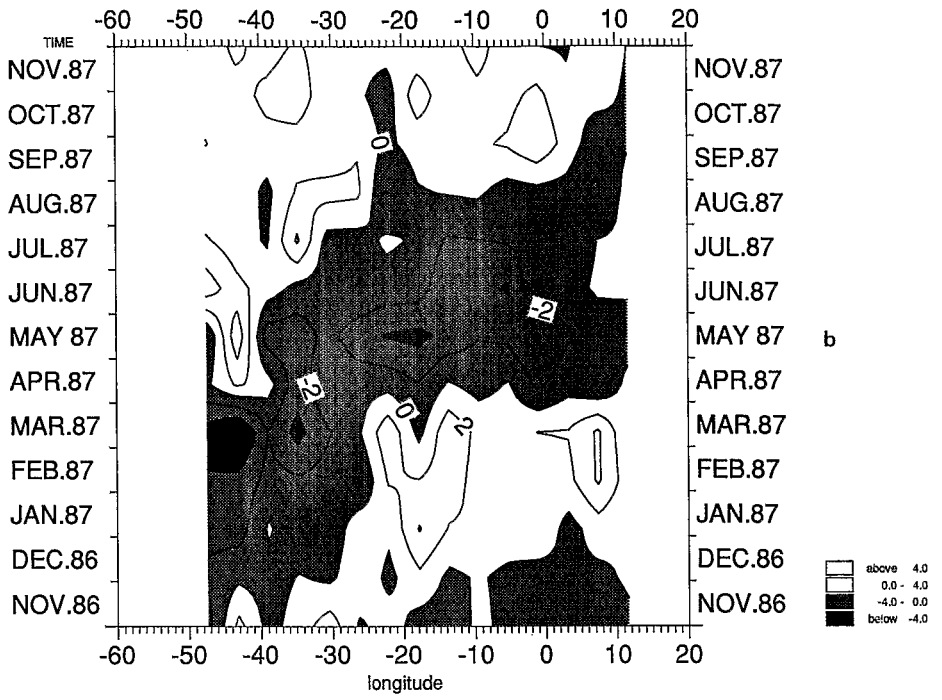

ALT. 1S

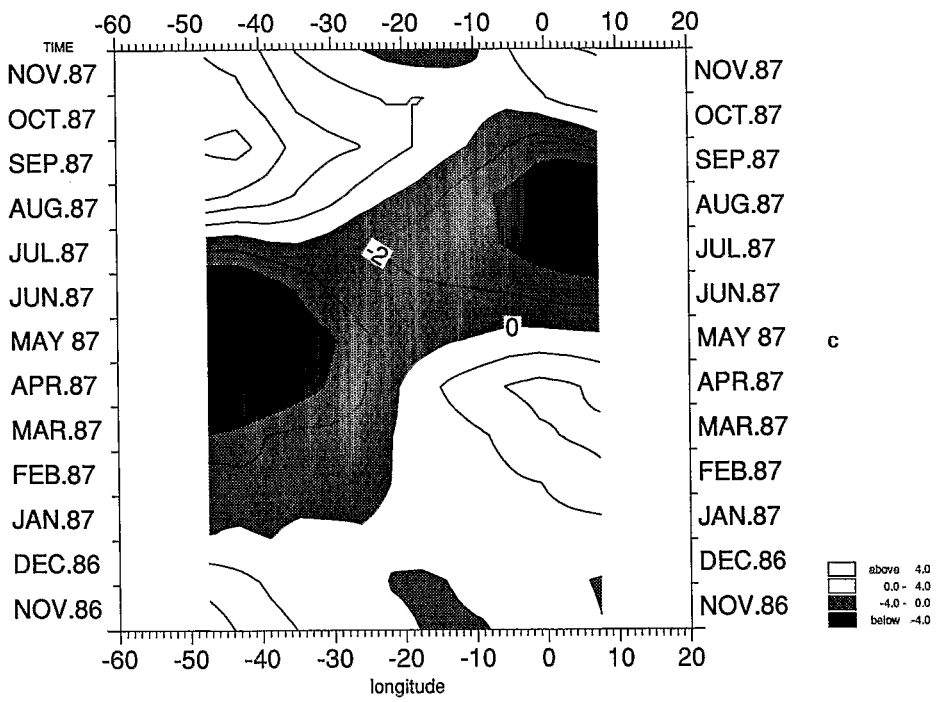

MODEL 1S

Fig. 19. (continued)

abnormal warm event in 1984 characterized by a huge change of the zonal equatorial DH slope.

The decomposition in vertical modes is obtained from a mean density profile, characteristic of the middle of the equatorial Atlantic Ocean (24°W). The vertical structure functions A_n are then solutions of

$$\frac{\partial}{\partial z}\left(\frac{1}{N^2}\frac{\partial A_n}{\partial z}\right)+\frac{A_n}{C_n^2}=0$$

with the boundary conditions at the surface ($z = 0$) and at the bottom ($z = -H$) of the ocean:

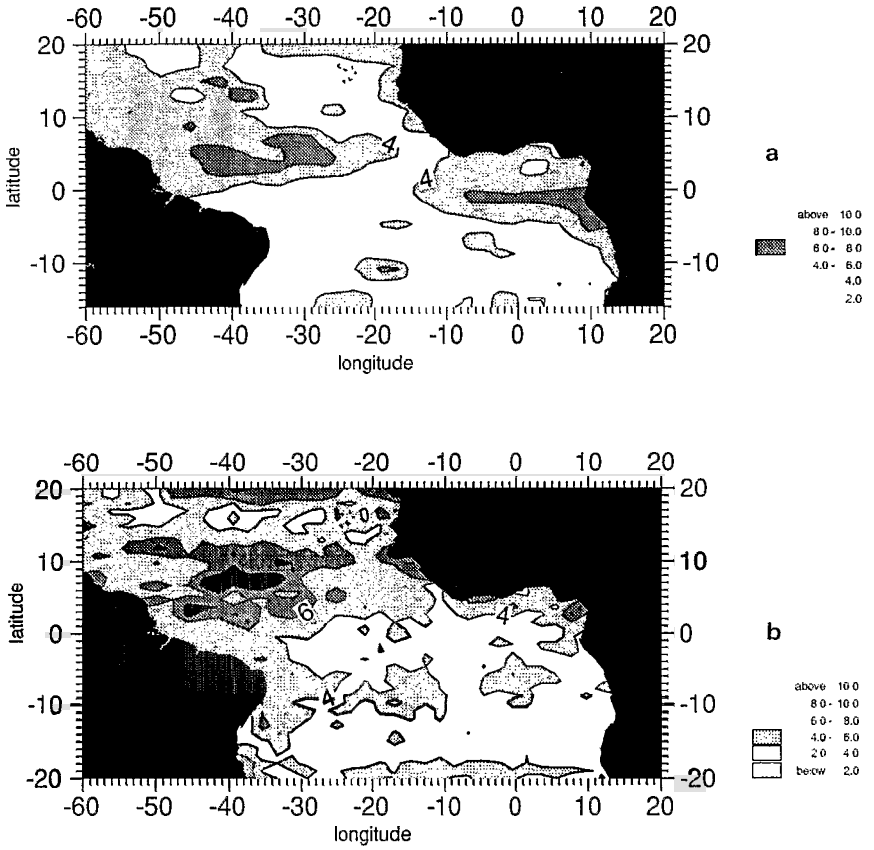

Fig. 20. Variability over the tropical Atlantic obtained (*a*) through DH data (in dynamic centimeters) and (*b*) through altimetric data from November 86 until November 87 (in centimeters).

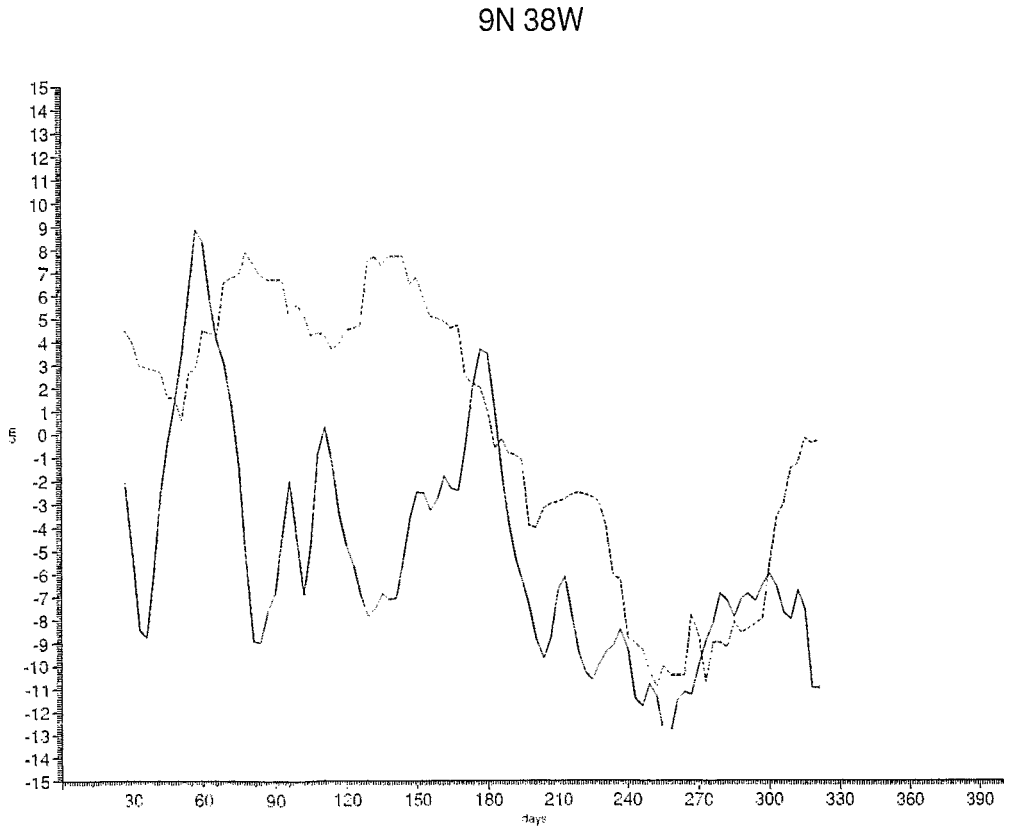

Fig. 21*a*. Comparison between IFS (solid line) and altimetry (dashed line) at 9°N, 38°W (in centimeters).

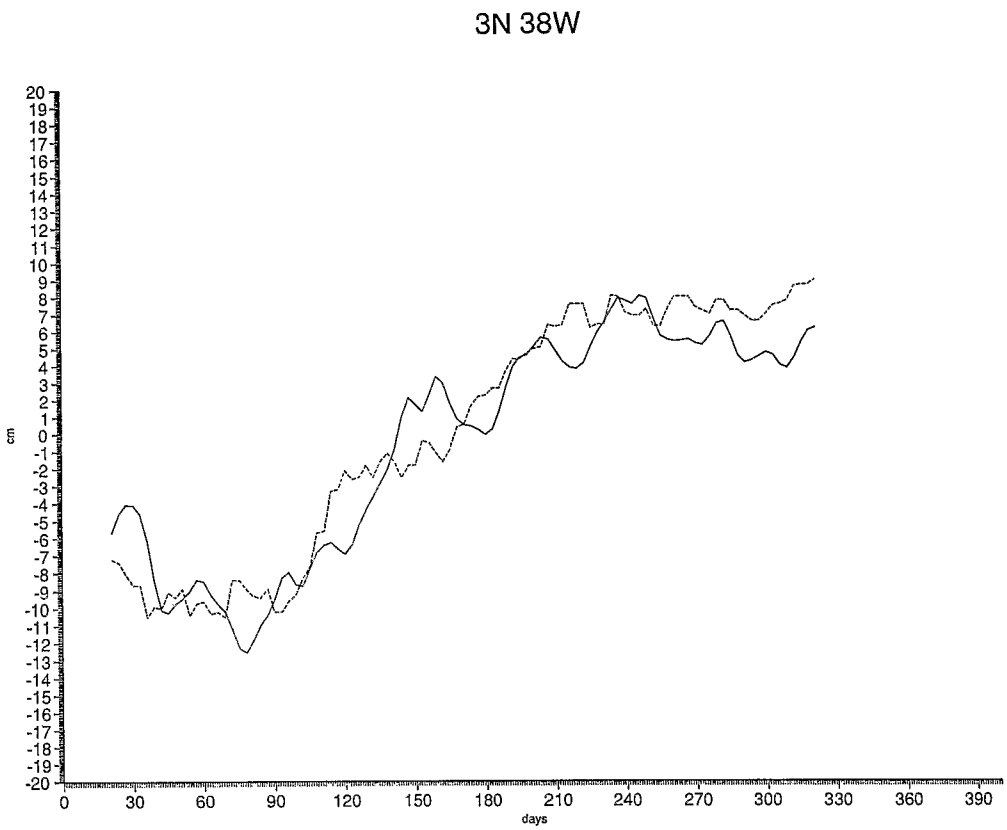

Fig. 21*b*. Same as Figure 21*a* except for 3°N, 38°W.

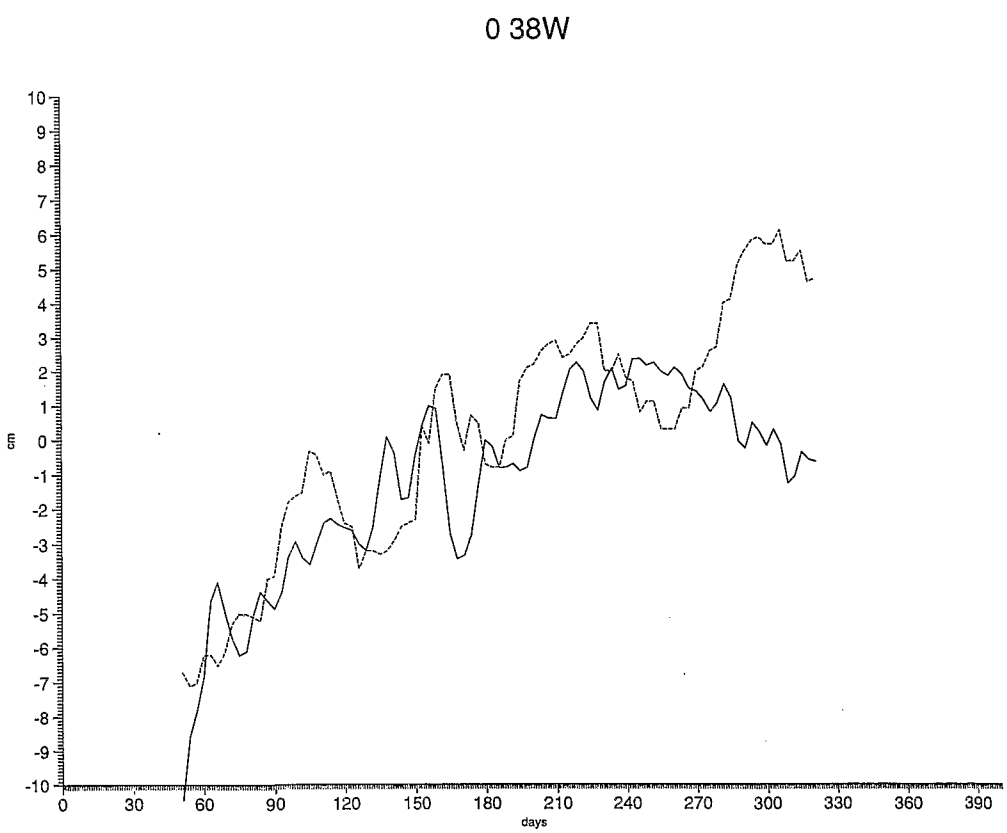

Fig. 21*c*. Same as Figure 21*a* except for 0°, 38°W.

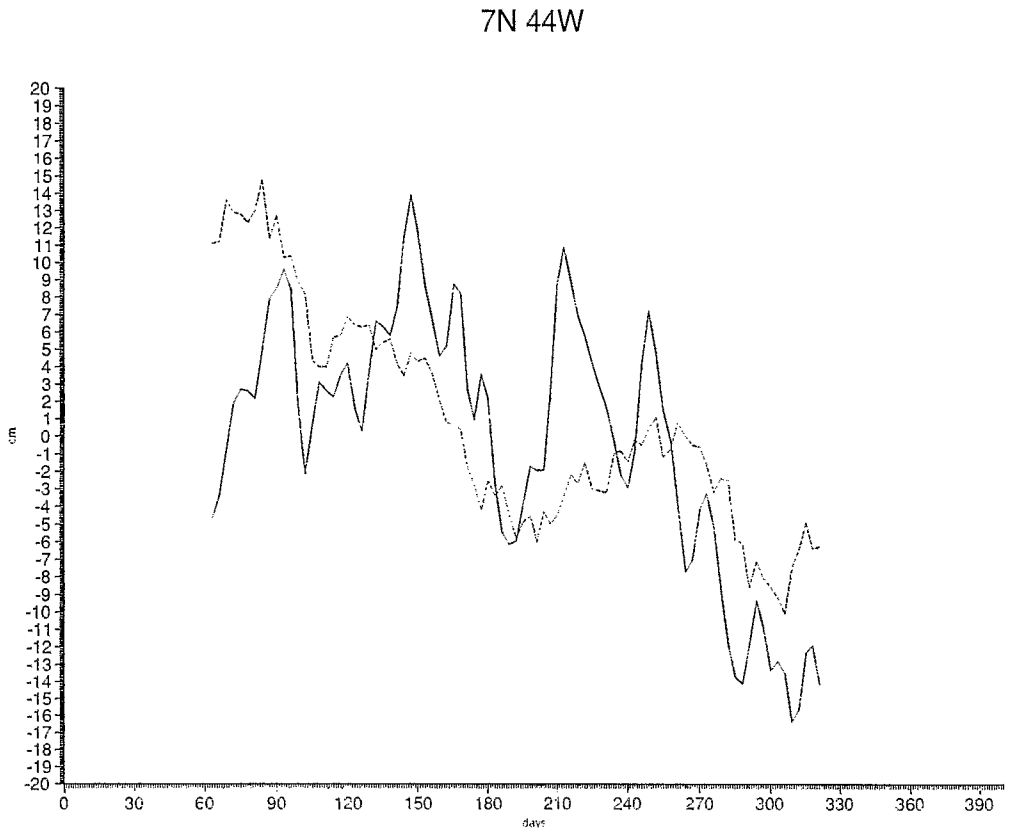

Fig. 21*d*. Same as Figure 21*a* except for 7°N, 44°W.

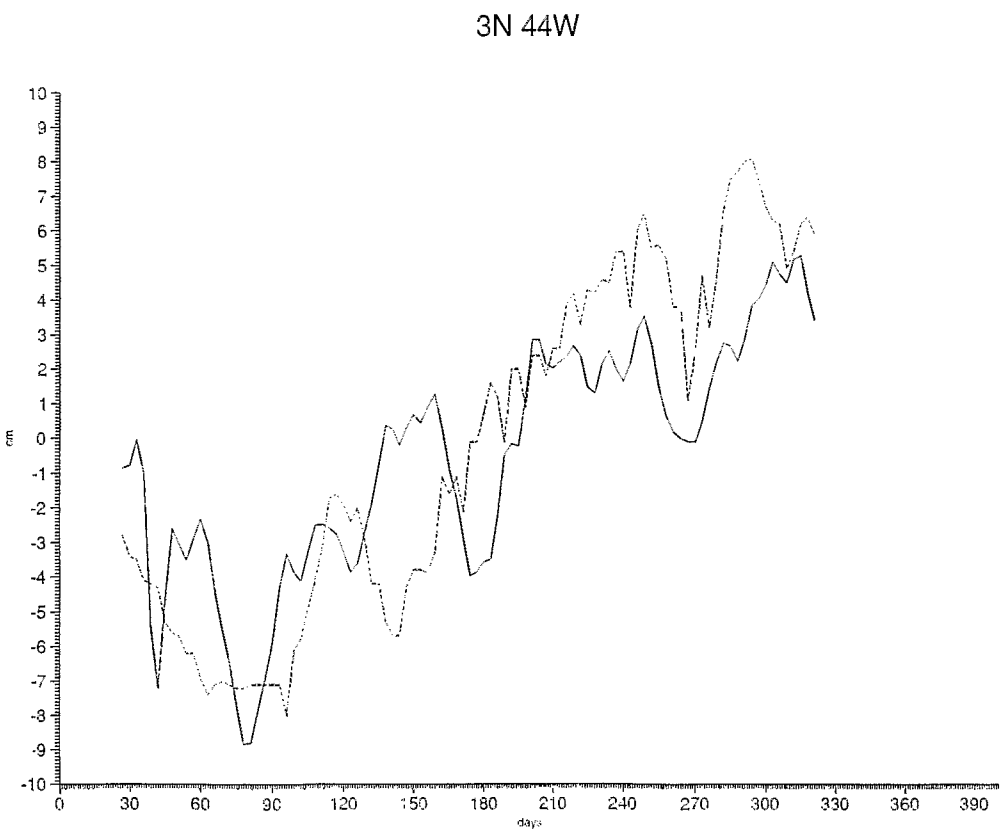

Fig. 21*e*. Same as Figure 21*a* except for 3°N, 44°W.

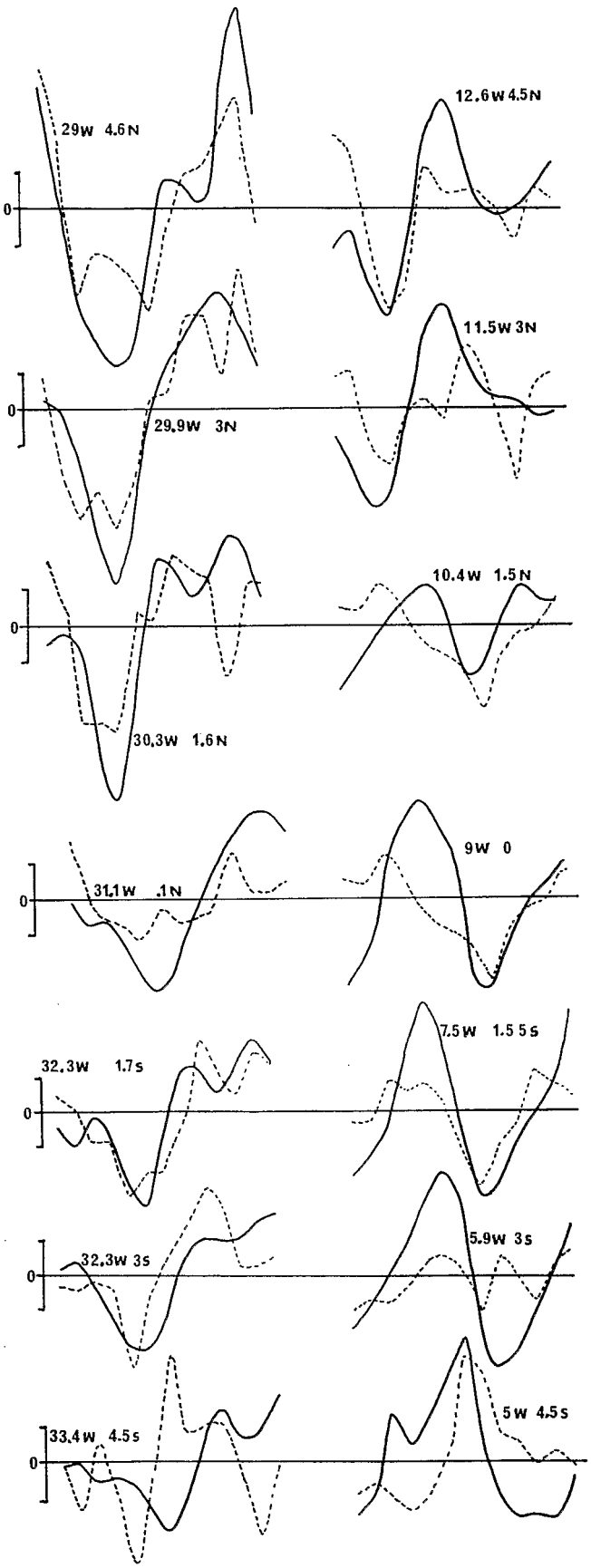

Fig. 22. Comparison between XBT-0/500 DH and altimetry along (left) Dakar–Rio de Janeiro and (right) Antilles-Cape Town ship lines between 5°N and 5°S. Units are dynamic centimeters and centimeters. The vertical scale is 2 (dyn) cm.

TABLE 2. Correlation Coefficients Between IES and Altimetric Data

	r_1	r	r_2
9°N, 38°W	0.20	0.36	0.49
3°N, 38°W	0.92	0.94	0.96
0°, 38°W	0.56	0.67	0.76
7°N, 44°W	0.41	0.55	0.66
3°N, 44°W	0.75	0.82	0.87

Also indicated are confidence intervals on the coefficient.

$$\frac{\partial A_n}{\partial z} = 0$$

where C_n is the phase speed associated to the mode n. The A_n functions are normalized so that

$$\frac{1}{H}\int_{-H}^{0} A_n^2(z)\, dz = 1$$

Then the horizontal velocity (U, V) and the pressure (P) fields can be written as the sum $(U, V, P)(x, y, z, t) = \Sigma_n (U_n, V_n, P_n)(x, y, t) A_n(z)$.

The horizontal equations are

$$\frac{\partial U_n}{\partial t} - fVn = \frac{1}{\rho_0}\frac{\partial P_n}{\partial x} + A_H \Delta_H U_n + F_n$$

$$\frac{\partial V_n}{\partial t} + fUn = -\frac{1}{\rho_0}\frac{\partial P_n}{\partial y} + A_H \Delta_H V_n + G_n$$

$$\frac{\partial P_n}{\partial t} + C_n^2\left(\frac{\partial U_n}{\partial x} + \frac{\partial V_n}{\partial y}\right) = 0$$

where

$$\Delta_H = \frac{\partial^2}{\partial x^2} + \frac{\partial^2}{\partial y^2}$$

and F_n, G_n are the horizontal projections of the forcing on each mode n:

$$F_n = \frac{\tau^x}{D_n} \qquad G_n = \frac{\tau^y}{D_n}$$

Values for C_n and D_n are given in Table 3 for the first three modes (only the first three modes are significantly excited).

These equations are discretized on a staggered grid (Arakawa type C) defined by trigonometric functions so that a variable grid spacing, depending on the area of interest, is obtained. The basin extends from 20°N to 20°S in latitude and from 60°W to 13°E in longitude. In longitude the smallest mesh size (50 km) is near the African and American coasts.

TABLE 3. Values for the First Three Vertical Modes of the Phase Velocity and Wind Coefficient Used in the Model

	C_n, cm/s	D_n, cm^{-1}
Mode 1	2.18	114,592
Mode 2	1.32	65,399
Mode 3	0.89	120,093

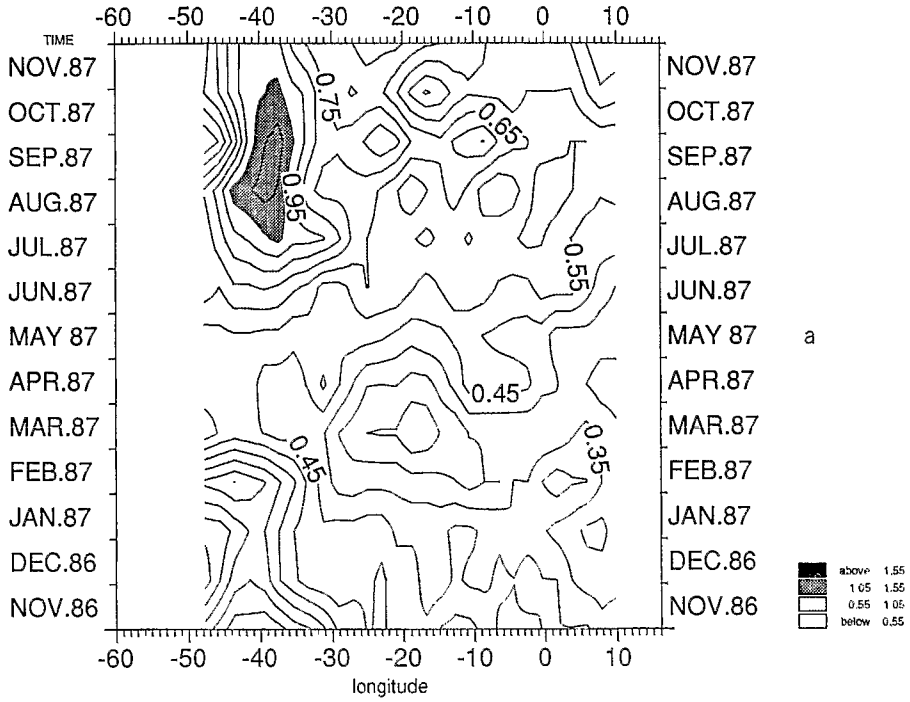

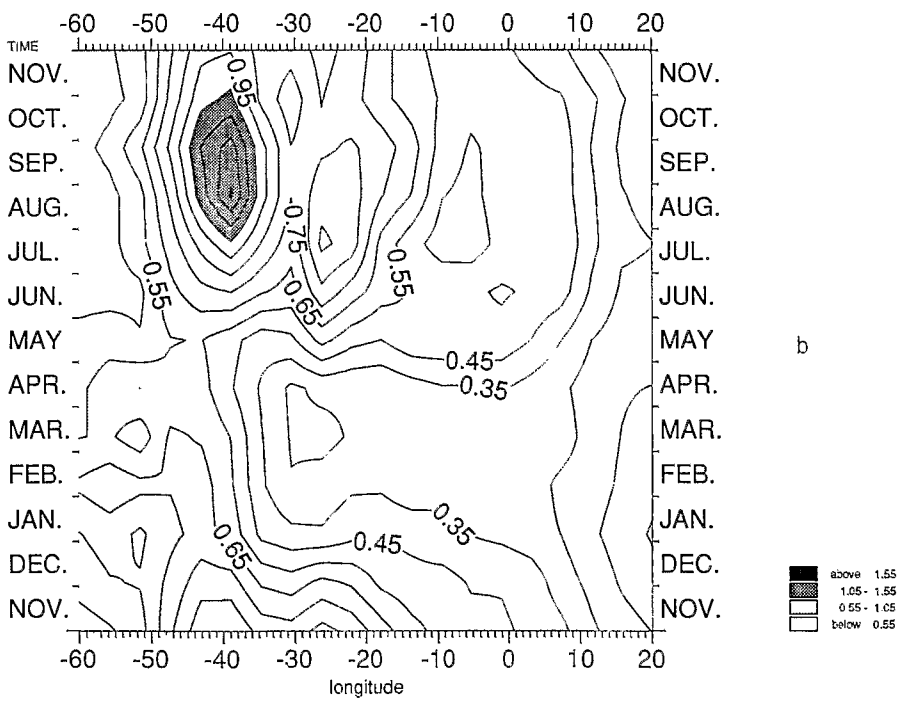

Fig. 23. Time evolution versus longitude between 2°N and 2°S of (*a*) Servain's wind stresses and (*b*) Hellerman and Rosenstein's wind stresses.

It increases to 115 km in the center of the basin. In latitude the smallest mesh size is at the equator (50 km) to correctly resolve the equatorial radius of deformation. At the northern and southern boundaries the mesh size is 85 km. No-slip boundary conditions have been used on the coastal, northern, western, and southern frontiers. The horizontal diffusivity coefficient (A_H) is 10^7 cm^2/s. A variable time step (1, 2, and 4 hours for first, second, and third modes, respectively) is incorporated for the time integration of the model. The model is spun up over 17 years by the *Hellerman and Rosenstein* [1983] climatological wind stress, then run with 1985–1988 monthly wind stress [*Servain et al.*, 1987].

The DH is obtained by

$$D = \int_0^{500} \frac{1}{\rho(s, t, p)}\, dp - \int_0^{500} \frac{1}{\rho(35, 0, p)}\, dp$$

$$D = D_r - D_0 + \sum_{n=1}^{3} P_n D_n$$

with

$$D_r = \int_0^{500} \frac{1 - H}{\rho_\Theta(p)}\, dp$$

$$D_0 = \int_0^{500} \frac{1}{\rho(35, 0, p)}\, dp$$

$$D_n = \int_0^{500} \frac{1 - H}{g\rho_\Theta^2(p)} \qquad P_n \frac{dA_n}{dz}$$

4.2. *Comparison of Altimetry With Model Results*

DH anomaly maps issued from the model simulation are given in Figures 2*c* to 14*c*. Mostly zonal structures are here again clearly identified. The signal is stronger in the northern hemisphere, where the low and high evolutions can be followed as was described before for altimetry and DH. In the region of the NEC (at 15°N; Figure 16*c* and in the region of the NECC (at 5°N; Figure 17*c*) the modeled signals are in good qualitative and quantitative agreement with the altimetric data (Figures 16*b* and 17*b*). Values are of the same order except that the eastern minimum at 5°N that occurs during boreal summer is stronger in the model. It is interesting to note that in the eastern part of the NEC (Figure 16), altimetry and model are in phase (negative values during the boreal winter-fall season) so that the out-of-phase evolution between altimetry and DH mentioned previously is probably due to an interannual event that characterizes the year 1987. At 1°N (Figure 18), both altimetric data and the model show similar evolution. East of 20°W, the negative upwelling modeled signal is obtained from mid-May 1987 until September 1987. So the model presents a 1987 upwelling starting at 1°N 1 month earlier than climatological DH, and ending also 1 month earlier. This is in better agreement with the altimetric signal. The order of magnitude of the signal amplitude is the same for altimetry and model west of 20°W but is different in the eastern part of the basin. These results are confirmed at 1°S (Figure 19) where the model produces negative values which are maximum in July–August 1987 instead of mid-May to July 1987 for altimetry. Thus even if the time shifting shown along the equator by altimetric data relative to DH is not fully explained by the model, it seems that the 1987 summer upwelling occurred earlier in the Gulf of Guinea and was weaker than usual.

5. DISCUSSION AND CONCLUSION

The comparison between DH and altimetric data has pointed out two major differences.

First, the amplitude of the altimetric signal is 2–3 cm lower than the DH amplitude. This could be due to the specific processing applied to the altimetric data in order to filter out all long-wave length errors (e.g., orbit error). This processing can also filter out a part of the ocean signal. A confirmation of this has been found by applying to DH data the same filter as the one applied to altimetry. We found that the DH signal is then reduced by about 15 to 25%.

A specific problem due to the FNOC wet tropospheric correction could also be responsible for a part of the differences. As was mentioned earlier, new SSM/I corrections will shed light on this for the future.

Another difference between altimetry observations and the DH climatology refers to the time shifting of oceanic seasonal events such as the equatorial upwelling which occurs earlier in the altimetry than in the climatology. In order to interpret these discrepancies, we ran a simple model over the period 1986–1987. We found that a large part of the discrepancy observed between the altimetric data and the DH climatology is due to the fact that climatology poorly represents the reality of the 1986–1987 period. This is especially true during summer 1987, when the equatorial upwelling, as revealed by model simulation and 1987 in situ data, occurs earlier in the Gulf of Guinea and was weaker than usual. This hypothesis of weak and early upwelling in the tropical Atlantic Ocean in 1987 has been also confirmed by sea surface temperature observations obtained from two distinct sources, in situ measurements (J. Servain, personal communication, 1988) and satellite observations [*Citeau et al.*, 1987], but a remaining time lag of about a month between altimetry and model upwellings for the period is still pending. Several explanations could be proposed. One of them is the lack of high-frequency energy in the winds used to force the model. These winds are obtained through an objective analysis [*Servain et al.*, 1987] with a climatological guess field. Unfortunately, in 1986–1988, wind data coverage was poor and important events may have been smoothed or even ignored. The wind stress evolution along the equator from November 1986 to November 1987 (Figure 23*a*) is quite similar to that described by *Hellerman and Rosenstein*'s [1983] climatology (Figure 23*b*) and seems to have missed some high-energy events. For example, the intensification of the easterlies in the western (25°–35°W) equatorial Atlantic, which is known to play an important role in the triggering of the equatorial upwelling [*Philander and Pacanowski*, 1986], begins in March–April 1987, or 1 month earlier than the climatology. However, this intensification seems to be too smooth compared with higher resolution data sets which present a rapid intensification of the wind along 28°W from March 1987 to June–July 1987 [*Citeau et al.*, 1987]. Thus with a better wind closer to reality we can expect to get from the model an even earlier upwelling in agreement with the Geosat observations.

Thus in conclusion, by comparison with climatological data, the altimetric data obtained between November 1986 and November 1987 from the Geosat altimeter are able to reproduce the large-scale signal observed in the tropical Atlantic Ocean. The agreement between altimetry and in situ data in the NECC region (around 5°N), where the seasonal signal has a maximum amplitude, is particularly good, especially between altimetry and 1987 IES records when the correlation between the two kinds of data sets is higher than 0.8. Comparison with the simulation of a simple model forced by monthly 1986–1987 wind stress strengthens this conclusion and emphasizes that observed differences are due mostly to interannual events such as a weak and early

summer upwelling in the Gulf of Guinea in 1987. Then the present state of the art in the use of altimeter observations in the tropics shows that the description of the large-scale, low-frequency variability of surface DH is possible. The altimeter observations seem to be already a better witness of the DH variability over a particular year than the climatological DH and with a much better resolution. This is a preliminary result from the first year of Geosat data. The new set of Geosat data covering several years, which will be available soon, will make it possible to better discriminate the interannual variability of oceanic sea level and, it is hoped, to better assess the quality and the usefulness of altimetry in the tropics.

Acknowledgments. The authors wish to thank E. J. Katz of the Lamont-Doherty Geological Observatory of Columbia University for providing IES data records (data were paid by a NSF grant) and G. Reverdin of the Laboratoire d'Océanographie Dynamique et de Climatologie (LODYC) in Paris for dynamic height values. Helpful comments from the modeling working group of LODYC were appreciated during the adjustment of the model, which was accomplished in collaboration with B. Bourles of the LODYC. Interesting discussions about altimetric data were carried out with the Groupe de Recherche en Géodésie Spatiale, and the numerical data processing code was established in collaboration with the PAVIE group in Toulouse. Thanks to J. Servain for providing the 1985–1988 wind stresses. S. Arnault and J. Merle were supported by ORSTOM and Y. Menard by CNES. This research was funded by Programme National Télédétection Spatiale.

REFERENCES

Arnault, S., Tropical Atlantic geostrophic currents and ship drifts, *J. Geophys. Res.*, *92*(C5), 5076–5088, 1987.

Busalacchi, A., and J. Picaut, Seasonal variability from a model of the tropical Atlantic Ocean, *J. Phys. Oceanogr.*, *13*, 1564–1588, 1983.

Cane, M. A., The response of an equatorial ocean to simple wind stress patterns, II, Numerical results, *J. Mar. Res.*, *37*(2), 253–299, 1979.

Cane, M., and T. Sarachik, The response of a linear baroclinic equatorial ocean to periodic forcing, *J. Mar. Res.*, *39*, 651–693, 1981.

Cartwright, D. E., and R. J. Taylor, New computations of the tide generating potential, *Geophys. J. R. Soc. London*, *23*, 45–74, 1971.

Cheney, R. E., J. G. Marsh, and B. D. Beckley, Global mesoscale variability from colinear tracks of Seasat altimeter data, *J. Geophys. Res.*, *88*, 4343–4354, 1983.

Cheney, R. E., B. C. Douglas, R. W. Agreen, L. L. Miller, and D. L. Porter, Geosat altimeter geophysical data record (GDR) user handbook, *NOAA Tech. Memo. NOS NGS-46*, 23 pp., Natl. Ocean Serv., NOAA, Rockville, Md., 1987.

Citeau, J., J. C. Berges, H. Demarcq, and L. Marec, Position de la zone intertropicale de convergence le long de 28°W et temperature de surface de l'océan, *Veille Clim.*, pp. 3–5, Sept. 1987.

De Mey, P., and A. R. Robinson, Simulation and assimilation of satellite altimeter data at the oceanic mesoscale, *J. Phys. Oceanogr.*, *17*, 2280–2293, 1987.

Douglas, B. C., R. E. Cheney, and R. W. Agreen, Eddy energy of the northwest Atlantic and Gulf of Mexico determined from GEOS 3 altimetry, *J. Geophys. Res.*, *88*, 9595–9603, 1983.

Du Penhoat, Y., and Y. Gouriou, Hindcasts of equatorial sea surface dynamic height in the Atlantic in 1982–1984, *J. Geophys. Res.*, *92*(C4), 3729–3740, 1987.

Du Penhoat, Y., and A. M. Treguier, The seasonal linear response of the tropical Atlantic Ocean, *J. Phys. Oceanogr.*, *15*, 316–329, 1985.

Emery, W. J., G. H. Born, D. G. Baldwin, and C. L. Norris, Satellite-derived water vapor corrections for Geosat altimetry, *J. Geophys. Res.*, *95*(C3), 2953–2964, 1990.

Fu, L., On the wave number spectrum of oceanic mesoscale variability observed by Seasat altimeter, *J. Geophys. Res.*, *88*, 4331–4342, 1983.

Garzoli, S., and E. Katz, The forced annual reversal of the Atlantic North Equatorial Countercurrent, *J. Phys. Oceanogr.*, *13*, 2082–2090, 1983.

Hellerman, S., and M. Rosenstein, Normal monthly wind stresses over the world ocean with error estimate, *J. Phys. Oceanogr.*, *13*, 1093–1104, 1983.

Hisard, P., and C. Hénin, Response of the Equatorial Atlantic Ocean to the 1983–1984 wind from the Programme Français Ocean et Climat dans l'Atlantique Equatorial cruise data set, *J. Geophys. Res.*, *92*(C4), 3759–3768, 1987.

Jourdan, D., C. Boissier, A. Braun, and J. F. Minster, Influence of wet tropospheric correction on mesoscale dynamic topography as derived from satellite altimetry, *J. Geophys. Res.*, this issue.

Katz, E., Sea surface response to wind in the equatorial Atlantic, *J. Geophys. Res.*, *92*(C2), 1885–1893, 1986.

Lass, H. U., V. Bubnov, J. M. Huthnance, E. J. Katz, J. Meincke, A. de Mesquita, F. Ostapoff, and B. Voituriez, Seasonal changes of the zonal pressure gradient in the equatorial Atlantic during the FGGE year, *Oceanol. Acta*, *6*, 3–11, 1987.

Leetmaa, A., and M. Ji, Operational hindcasting of the tropical Pacific, *Dyn. Atmos. Oceans*, in press, 1989.

Malarde, J. P., P. De Mey, C. Perigaud, and J. F. Minster, Observation of long equatorial waves in the Pacific Ocean by Seasat altimetry, *J. Phys. Oceanogr.*, *17*, 2273–2279, 1987.

Menard, Y., Observation of eddy fields in the northwest Pacific by Seasat altimeter data, *J. Geophys. Res.*, *88*, 1853–1866, 1983.

Menard, Y., Observing the seasonal variability in the tropical Atlantic from altimetry, *J. Geophys. Res.*, *93*(C11), 13,967–13,978, 1988.

Merle, J., Seasonal heat budget in the equatorial Atlantic Ocean, *J. Phys. Oceanogr.*, *10*, 464–469, 1983.

Merle, J., and S. Arnault, Seasonal variability of the surface dynamic topography in the tropical Atlantic Ocean, *J. Mar. Res.*, *43*, 267–288, 1985.

Merle, J., M. Fieux, and P. Hisard, Annual signal and interannual anomalies of SST in the eastern equatorial Atlantic Ocean, *Deep Sea Res.*, *26*, GATE suppl. 2–5, 77-102, 1979.

Miller, L., R. E. Cheney, and D. Milbert, Sea level time series in the equatorial Pacific from satellite altimetry, *Geophys. Res. Lett.*, *13*, 475–478, 1986.

Monaldo, F., Path length caused by atmospheric water vapor and their effects on the measurement of mesoscale ocean circulation features by a radar altimeter, *J. Geophys. Res.*, *90*(C3), 2923–2932, 1990.

Morlière, A., G. Reverdin, and J. Merle, Assimilation of temperature profile in an OGCM for a continuous survey of tropical Atlantic, *J. Phys. Oceanogr.*, *19*(12), 1892–1899, 1989.

Musman, S., Sea slope changes associated with westward propagating equatorial temperature fluctuations, *J. Geophys. Res.*, *91*(C9), 10,753–10,757, 1986.

Perigaud, C., J. F. Minster, and G. Reverdin, Zonal slope variability of the tropical Indian Ocean studied from Seasat altimetry, *Mar. Geod.*, *10*, 53–67, 1986.

Philander, S. G. H., and R. C. Pacanowski, A model of the seasonal cycle in the tropical Atlantic Ocean, *J. Geophys. Res.*, *91*(C12), 192–206, 1986.

Reverdin, G., and Y. Du Penhoat, Modelled surface dynamic height in 1964–1984: An effort to assess how well the low frequencies in the equatorial Atlantic were sampled in 1982–1984, *J. Geophys. Res.*, *92*, 1899–1913, 1987.

Richardson, P. L., and T. McKee, Average seasonal variation of the Atlantic equatorial currents from historical ship drifts, *J. Phys. Oceanogr.*, *14*, 1226–1238, 1984.

Richardson, P. L., and G. Reverdin, Seasonal cycle of velocity in the Atlantic North Equatorial Countercurrent as measured by surface drifters, current meters, and ship drifts, *J. Geophys. Res.*, *92*, 3691–3708, 1987.

Saastamoinen, J., Atmospheric correction for the troposphere and stratosphere in radio ranging of satellites, in *The Use of Artificial Satellites for Geodesy*, *Geophys. Monogr. Ser.*, vol. 15, edited by S. W. Henriksen et al., pp. 247–251, AGU, Washington, D. C., 1972.

Schwiderski, E. W., On charting global tides, *Rev. Geophys.*, *18*(1), 243–268, 1980.

Servain, J., M. Seva, S. Lukas, and G. Rougier, Climatic atlas of the tropical Atlantic wind stress and sea surface temperature: 1980–1984, *Ocean-Air Interact.*, *1*, 109–182, 1987.

Tapley, B. D., J. B. Lundberg, and G. H. Born, The Seasat altimeter wet tropospheric range correction, *J. Geophys. Res.*, *87*(C5), 3213–3220, 1982.

S. Arnault and J. Merle, Laboratoire d'Océanographie et de Climatologie ORSTOM, Université Pierre et Marie Curie, Tour 14-2, 4, Place Jussieu, 75252 Paris Cedex 05, France.

Y. Menard, Groupe de Recherche en Géodésie Spatiale, CNES, 18 avenue Belin, 31055 Toulouse Cedex, France.

(Received June 3, 1989;
accepted December 28, 1989.)